Research Report

_____

Investigation into the use of variable speed drives to damp mechanical oscillations

_____

Author: *Supervisor:*

Greg Blaski   *Dr. John Van Coller*
Student Number: 0216843H

School of Electrical and Information Engineering

Declaration of Authorship

I hereby certify that this Research report has been composed by me and is based on my own work, unless stated otherwise. No other person's work has been used without due acknowledgement in this Research report. All references and verbatim extracts have been quoted, and all sources of information, including graphs and data sets, have been specifically acknowledged. All images used in the report which were sourced from textbooks and journals have been used with the written permission from the respective publisher and/or author in each case. The copyright clearance certificates and the respective author's written permission can be found in the Appendix of the report.

Date:___**08/06/2016**_____

Signature:_____

" The difference between a master and an apprentice? The master has failed more times than the apprentice has even tried"

<p align="right">*- Stephen McCranie*</p>

Abstract

An investigation was conducted into how a variable speed drive can provide a damping torque when mechanical oscillations are present. The modeling of mechanical oscillations via an analogous electrical circuit was performed. Simulation was used to demonstrate how a variable speed drive is able to damp speed oscillations using Direct Torque Control (DTC). Damping of mechanical oscillations is done by means of the variable speed drive providing a damping torque component that is in-phase with the speed deviation. The simulation showed that by applying a small torque component with the speed variation results in torque oscillations being damped by 60% after the initial disturbance. Damping is further improved by applying a torque component equal to the speed variation resulting in the oscillations being damped by 80% when compared to the initial disturbance.

Acknowledgements

Contents

List of Figures

List of Tables

Abbreviations

VSD   **V**ariable **S**peed **D**rive

DTC   **D**irect **T**orque **C**ontrol

LCI   **L**oad **C**ommutated **I**nverters

ITMD   **I**ntegrated **T**orsional **M**ode **D**amping

TNF   **T**orsional **N**atural **F**requency

PWM   **P**ulse **W**idth **M**odulation

SF   **S**ervice **F**actor

SVM   **S**pace **V**ector **M**odulation

ESR   **E**quivalent **S**eries **R**esistance

1   Introduction

The oil and gas industry has a growing demand for Variable Speed Drives (VSDs). Advantages of a VSD are an increase in operational flexibility and energy savings. Mechanical loads coupled to a VSD can experience torsional vibrations. A torsional vibration is an oscillatory variation in the twist in certain shaft sections [1]. A possible consequence of uncontrolled torsional vibrations is mechanical damage to the motor and mechanical load.

The research topic will involve modeling a VSD driving a motor, with a load connected the motor. The motor shaft connects via rigid coupling, to the shaft of a mechanical load. The mechanical load after the coupling, i.e. a fan, exhibits mechanical oscillations (the torsional vibrations described above). Electrical and mechanical analogues will be derived, followed by the derivation of a rotational system. The rotational analogue is applied to a wind turbine application and how damping is achieved following a disturbance. An investigation will be done on how the VSD can provide damping of these torsional vibrations (via Matlab simulations).

Before approaching the simulation in the research report, mechanical modeling of a mechanical shaft and a detailed discussion on the theory behind drive control technologies using Direct Torque Control (DTC) will be done to give an idea on what is occurring in the background of the simulation. Before the literature survey and report begins, an outline of what is to be achieved is briefly discussed.

1.1   Objectives of the Research report

The aim of this research report will involve investigating how a VSD can be utilized to achieve the damping described. In addition, the research report will attempt to answer three questions concerning the VSD and motor control system, these questions include:

➢ Can a VSD provide damping for oscillations associated with its mechanical load?

➢ What types of mechanical oscillation can be damped?

➢ Will providing damping have a detrimental effect on the VSD-mechanical load performance?

Once the theory of the control technology using DTC is presented, a simulation will be done via Simulink to demonstrate how such damping is performed via a VSD. Upon completion of the simulation, the above questions can then be answered when the results are analyzed.

2   Literature Review

There have been a number of industry studies on the problem of torsional vibrations for a mechanical load coupled to a VSD, with numerous methods proposed to counter these torsional vibrations. Load Commutated Inverters (LCI) are often used to drive large gas compression trains. An improvement in efficiency comes at the expense of torque harmonics resulting from the current harmonics produced by the power electronic converter [1]. These torque harmonics can often excite mechanical resonances in the mechanical load.

One technique used to limit torsional vibrations is referred to as Integrated Torsional Mode Damping (ITMD). This method is based on a torsional vibration measurement in the mechanical load with an interface to the existing inverter controller. In order to implement damping, the DC link inductors of the LCI are used for temporary energy storage. The damping controller reacts to torsional vibrations by using this source of stored energy to allow the modulation of the power flow into and out of the motor without negatively impacting the performance of the system [1].

In terms of measurement, standard equipment used for lateral vibration (i.e. accelerometers) is not able to accurately measure these vibrations. The torsional vibration is dependent on the stiffness of the motor shaft with motor couplings also playing a role. Tests have shown that in order to accurately measure the torsional vibrations, shaft torque needs to be monitored by use of a full-bridge strain gauge system with telemetry [1]. An additional example of a sensing system is a continuous duty torque meter.

A drawback of such a system is that it would need to be integrated in the mechanical load, typically during the design phase since adding one later can be a costly exercise.

The ITMD system is an electro-mechanical damping method integrated with the electrical drive control. It was developed to assist in making turbo machinery less sensitive to motor driven torque harmonics [1]. A block diagram of a typical system is shown in Figure 1.
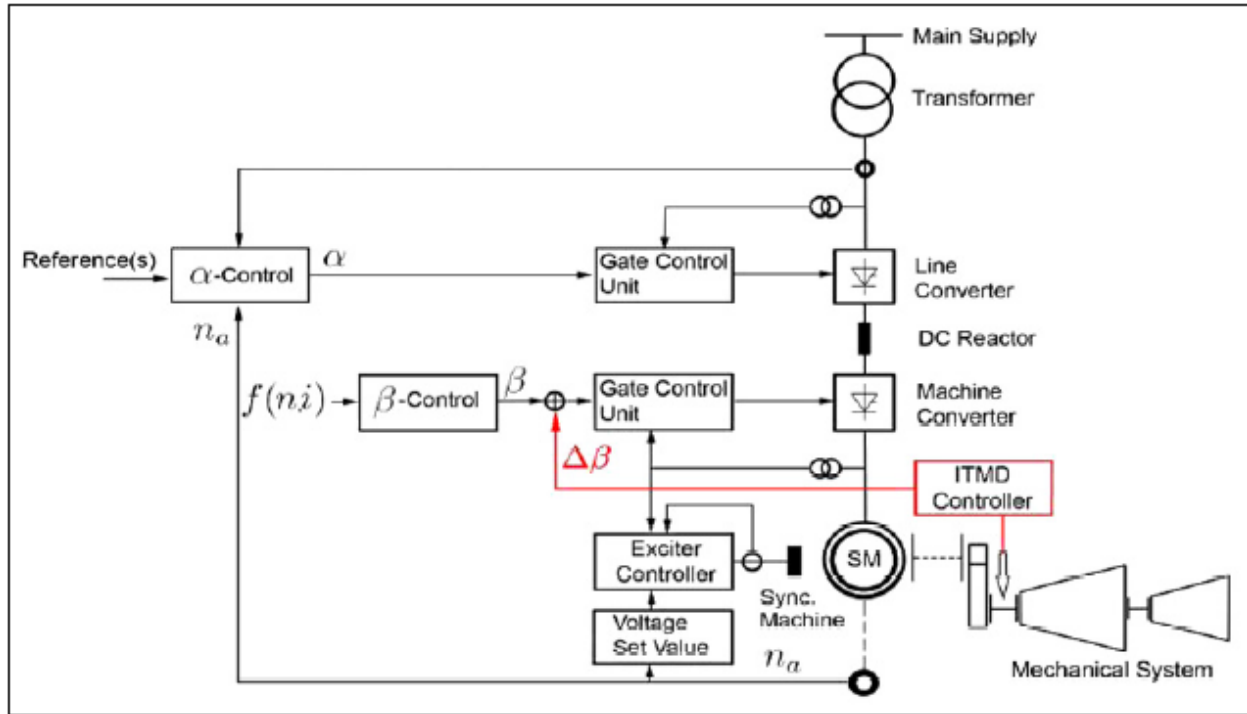
Figure 1: Typical block diagram of an LCI drive system with integrated ITMD control [1].
Image used with publisher permission, Copyright © 2010, IEEE.

From the block diagram in Figure 1, the line converter is controlled by means of the firing angle which executes the closed loop functions (i.e. speed control of the VSD via torque control). By adding a small signal modulation of Δβ, to the input signal to the Gate Control Unit, ITMD control can be obtained. This modulation signal implements damping by generating an additional air-gap torque component with a frequency that is identical to the torsional natural frequency of the mechanical load [1].

The aim of the damping control is not to totally suppress a torsional vibration, but to keep the torsional vibrations at such a level that the stresses are kept within safe operating limits. An example of torsional mode damping is demonstrated in Figure 2 of the block diagram described in Figure 1. The figure describes a simulated effect of torsional mode damping for a 30 MW natural gas compression train [1]. It can be seen from the diagram that when the ITMD mode is activated damping of the mechanical oscillations increases.

The effectiveness of such a system is dependent on several factors. Such factors can include accuracy of calculated mechanical parameters, accuracy of the estimated pulsating torque components caused by the drive system, inter-harmonic interactions caused by other VSD loads connected to the same power system and, in the case of a turbine system, dynamic torque components caused by aerodynamic effects.

To further investigate mechanical resonance, the interaction between the VSD and the mechanical load would need to be measured under laboratory conditions.
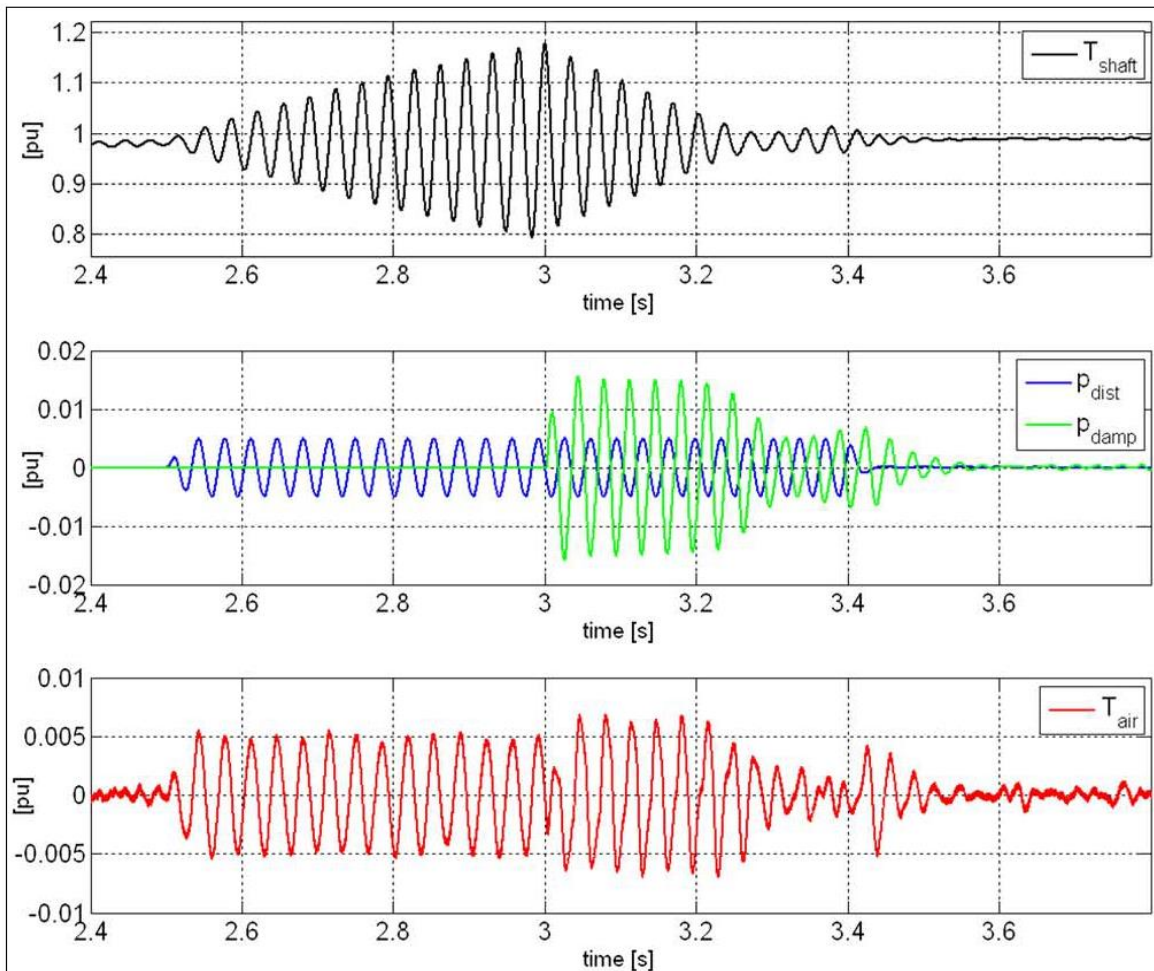
**Figure 2: Simulated effect of torsional mode damping for a 30 MW compression train [1].
Image used with publisher permission, Copyright © 2010, IEEE.**

For large drives, such vibrations can lead to added fatigue stress and would need to be minimized as even an hour of downtime can be expensive. Further studies done on a compressor unit utilizing a system referred to as DriveMonitor[TM] [2] found that significant levels of oscillations were visible at a frequency independent of rotational speed and loading with the oscillation frequency associated with a mechanical resonance [2]. A compressor is only one example of machines that are susceptible to torsional vibrations. Other machines that are susceptible include rolling mills and paper machines [2].

A particular study found that oscillations may appear or disappear as a result of process disturbances which can be caused by set point changes. It was observed that the frequency of observed oscillations is independent of the rotational speed of the motor [2]. This eliminates the possibility of the oscillations resulting from mechanical imbalances.

An alternative technique for observing mechanical resonance is to observe the machine operation at different speeds. This information is then presented in a form known as a Campbell diagram. VSDs produce torque harmonics with frequencies that are multiples of the fundamental output frequency. These torque harmonics can excite mechanical resonances that are clearly visible. An example of the Campbell diagram applied to the compressor is shown in Figure 3.
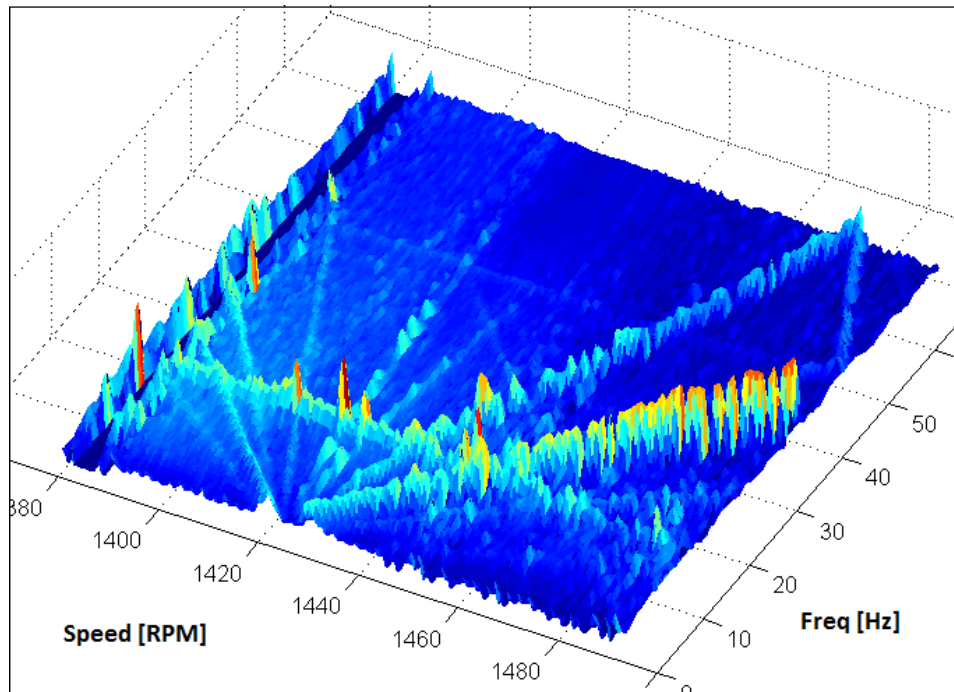
Figure 3: Campbell diagram for a compressor driven by an electric motor [2].
Image used with publisher permission, Copyright © 2011, IEEE.

The vertical axis in the Campbell diagram is the dynamic torque vibration amplitude at the respective frequency and RPM value. The torque amplitude is normally expressed in kN.

The mechanical components of the compressor plus motor can be modeled in the form of the simple mechanical system shown in Figure 4. This simple model recreates the first mechanical resonant mode behavior when the VSD responds dynamically to a change in set point. The study also showed that from the mechanical analysis, the torsional vibrations appear in the system when insufficient damping is present.

By modifying the mechanical system configuration (i.e. introducing active attenuation of the mechanical oscillations) the damping can be increased [2].

5
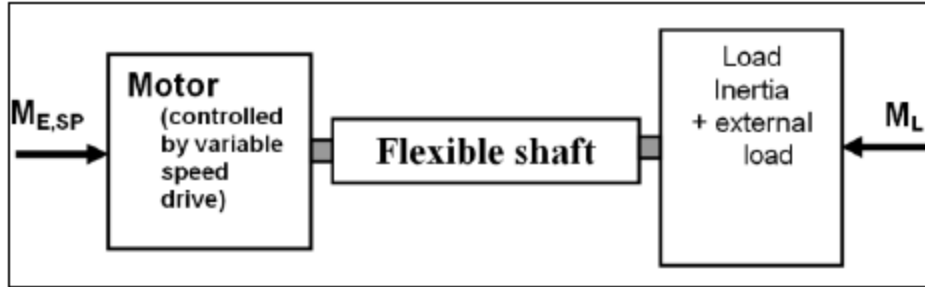
Figure 4: Simple model of the mechanical system [2].
Image used with publisher permission, Copyright © 2011, IEEE.

In order to test for these torsional vibrations on a smaller scale, a 5.5 kW motor with an ABB ACS800 inverter was used. The control algorithm was formulated utilizing Matlab and Simulink. Through the small scale test it was found that the test rig was able to provide a significant level of torsional vibration, such that the methods of torsional vibration detection and damping could be tested [2].

In the one such test, the drive was run with a constant speed set point. For this configuration, the mechanical resonance may only be excited by the switching of the VSD.

Other studies have used the method of modal analysis in order to determine the natural frequencies [3]. In such analysis, the driveline is modeled as discrete moments of inertia connected with inertia-free elastic elements that represent the shafts and couplings.

In the study it was quite common to find a deviation from the calculated frequency of between 20-30% [3]. The same study also found that when a VSD is connected to the system, there was a larger risk at a speed where a disturbance could result in resonance. However, most VSDs can improve damping by controlling the torque accordingly [3].

With the literature survey in hand, the sections that follow from this point in the research project will build upon what has been researched previously.

3   Mechanical and Torsional analysis

Building upon the previous discussion, the modeling of a mechanical shaft will be investigated. This section will discuss the equations for a 2-mass torsional system in addition to a Torsional Natural Frequency (TNF) equation. The TNF will be discussed further in a case study involving a VSD with torsional vibrations.

Many mechanical systems, be it fixed speed or driven by a VSD, will exhibit some form of vibration [4]. With the ever increasing speeds in motors and increased improvements to controller performance, the problem of resonance will increase as well. The vibration level of a mechanical system (be it a motor, load or shaft) is the result of imposed cyclic forces which can originate from a residual imbalance of the rotor, or from some other cyclic force and the response of the system to these forces [4]. The problems these forces create can be categorized as follows:

- High power, high speed applications where operation above the first critical speed is a requirement. The critical speed is defined as the theoretical angular velocity that excites the natural frequency of a rotating object, such as a shaft. As the speed of rotation approaches the object's natural frequency, the object begins to vibrate. If the shaft is accelerated quickly past its critical speed , there may not be enough time for shaft resonance to be established;
- Applications where a torque ripple excites a resonance in the mechanical system;
- High performance closed loop applications where the change of motor torque can be very high. This quick change in torque would subject the shaft linking the mechanical parts to a twisting action, where the control system tied to the motor would need to damp the vibration [4].

It should be noted that torque ripple produced by modern variable speed drives is relatively small when compared to earlier technology.

3.1   Modeling the torsional natural frequency equation

Any system that has masses or inertias that are coupled together via flexible elements is capable of producing mechanical vibrations. This section describes how a motor and load can be represented as a 2-mass torsional system with the TNF equation then being defined for the system. The torsional systems of the two masses are described by a simple model in Figure 5.
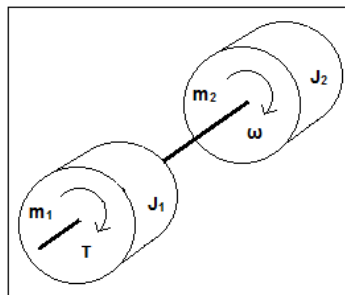
Figure 5: A two mass torsional system [4].

If one were to assume zero damping for the torsional system shown in Figure 5, the equations of motion can be defined as follows [4]:

$$J_1(d^2\theta_1/dt^2) + K(\theta_1 - \theta_2) = 0 \qquad (1)$$

$$J_2(d^2\theta_2/dt^2) + K(\theta_1 - \theta_2) = 0 \qquad (2)$$

The K term in the above two equations represents the torsional stiffness, which can be replaced with the term $\frac{GJp}{L}$. Where G is the shear modulus of elasticity, in Pa, J_p is the polar moment of inertia of the shaft, in kg-m^2, which can be equated to $\frac{r_4}{2}$ for a circular shaft of radius r, in m, and the shaft length being twisted as L, in m. From the two equations, eliminating θ_1 and θ_2 provides the following equation,

$$\theta = A + Bt + C\cos(\omega_{TNF} + \Phi) \qquad (3)$$

From the above equation, the TNF equation can be described as follows:

$$\omega_{TNF} = \sqrt{\frac{GJp}{L} \left[\frac{(J_1+J_2)}{(J_1 \cdot J_2)}\right]} \qquad (4)$$

The equation can be further expanded to produce a final TNF equation defined as follows.

$$f_{TNF} = \frac{1}{2\pi} \sqrt{\frac{GJp}{L} \left[\frac{(J_1+J_2)}{(J_1 \cdot J_2)}\right]} \qquad (5)$$

From the above equations, ω_{TNF} is the TNF in radians/sec while f_{TNF} is the TNF in Hz.

3.2   Shaft vibrations independent of VFDs

When one needs to determine if the vibrations are the result of the VSD or another part of the system, the drive can be ruled out by re-programming the VSD to run as a soft starter. This is achieved by reconfiguring the drive to only limit inrush currents such that the VSDs functionality is bypassed, and example of this will be presented in a case study. If torsional vibrations are still present, the drive is not the cause of the vibrations and other causes can be investigated. Torsional vibrations can be categorized as follows [4]:

- Sub-synchronous vibrations: Vibration frequencies below the shaft rotational frequency;
- Synchronous vibrations: Vibration frequency at the shaft rotational frequency;
- Super-synchronous vibrations: Vibration frequencies above the shaft rotational frequencies, and;
- Vibrations occurring at shaft critical speeds.

3.2.1 Sub-synchronous vibrations

The most common cause of this is for induction motors where beating at slip frequency can occur [4]. All electromagnetic forces in an induction motor occur at frequencies equal to, or at a multiple of, the supply frequency. The rotational speed is slightly less than synchronous speed [4]. Mechanical imbalances will produce vibration related to the rotational speed of the motor. Two cyclic forces at relatively close frequencies will combine to give a low frequency beat. If the motor itself has a broken rotor bar, vibration at the slip frequency will increase [4]

3.2.2 Synchronous vibrations

The most common cause of this vibration at the shaft rotational speed is a mechanical imbalance, or shaft misalignment. The mechanical imbalance may often be a specification or manufacturing quality issue. However, in larger motors, shaft bending can be attributed to uneven cooling of the shaft or overheating of the rotor in general [4]. Vibration due to thermal issues may get drastically worse over time, which can be noticed by a gradually increasing vibration over the life of the motor [4].

3.2.3 Super-Synchronous vibrations

Super synchronous vibrations are associated with out-of-round bearings or shaft asymmetry along its length. A possible cause can be the result of wearing of roller bearings. Similar scenarios can occur with synchronous vibrations where the vibrations will gradually increase over time due to wear, but as wear increases unchecked, it can lead to sudden catastrophic failure of a motor [4].

3.2.4 Critical speeds

With the aid of a VSD it is possible to increase the speeds of motors past their first and second critical speeds [4]. The critical speed of a shaft is not only dependent on the characteristics of the shaft, but is also affected by the stiffness of the bearing supports.

It is important to note that the magnitude of the shaft and bearing vibration is dependent on the resonance curve of the shaft, such that the closer it runs to the critical speed, the more intense the vibration level [4].

3.3 Resonance excitation from torque ripple

Problems with torque ripple are an inherent issue in almost all VSD applications [4]. The frequency of the torque ripple and the exact magnitude are dependent on the type of converter and the specific application. A DC motor fed from a six pole converter is considered as an example. The resultant motor armature current has a ripple at six times the mains frequency [4] such that for a 50 Hz supply the ripple has a fundamental frequency of 300 Hz. The magnitude of the torque ripple is on average 10-20% of the rated torque. The frequency of the torque ripple is a function of the mains frequency and not the running speed [4]. If the stated fundamental frequency of 300 Hz is not too close to the natural resonant frequency of the system, it should pose little risk to the mechanical system.

Torque ripple due to the commutation process in the DC motor is an important factor to consider when a small number of commutator segments is used. It will be this torque ripple that has a frequency component that is proportional to speed [4]. With a Pulse Width Modulated (PWM) converter, torque ripples at six and twelve times the output frequency could be of concern.

Looking again at the equations of motion for the two-mass system described earlier, when considering the torsional vibrations and observing the relative displacement of one body to the other, the following equation is obtained.

$$J\left(d^2\theta_1/dt^2\right) + \frac{GJ_p}{L}\theta = 0 \tag{6}$$

Introducing a driving force $r(t)$, the differential equation of the system can be obtained by applying the drive force into the above equation, which becomes the following.

$$J\left(d^2\theta_1/dt^2\right) + \frac{GJ_p}{L}\theta = r(t) \tag{7}$$

If the driving force can be represented by $r(t) = F\cos(\omega t)$ the equation will then appear as follows:

$$\theta(t) = \left[\frac{GJ_p}{L}\right]^2 \cos(\omega_o - \delta) + \left[\frac{F}{\left(\frac{GJ_p}{L}\right)_1\left[1-\left(\frac{\omega}{\omega_o}\right)^2\right]}\right]\cos(\omega t) \tag{8}$$

This equation represents the superposition of two oscillations. The first frequency is the natural frequency of the system, $\frac{\omega_o}{2\pi}$, while the second frequency is the frequency of the input force [4]. From the equation, the amplitude of the oscillation depends on the frequencies ω and ω_o. As the input frequency, approaches the natural frequency ω_o, resonance in the system will occur.

3.3.1 Methods of vibration reduction

During the operation of a motor, vibrations in the system will most likely be present no matter what precautions are taken. While it may not be entirely possible to eliminate resonances at critical speeds, they can be minimized to tolerable levels. The methods used to reduce noise and vibration can be summarized by the following points [4]:

- Improving the balancing and stiffening to reduce the amount of vibration. It is important that the alignment of rotating parts in the system is done accurately;

- Utilizing isolation to prevent vibrations from being transmitted. System solutions can include rubber mats and custom dampening devices to offer specific stiffness in various directions;

- Utilizing non-linear de-tuner type torsional couplings;

- Increasing the stability of the foundations, thus ensuring vibrations are not transmitted to the structure. It should be noted that the foundation calculation is done on a case by-case basis which plays a vital role in the installation process, and;

- With a VSD connected to the system it is possible to utilize the advanced functionality of the drive by utilizing the drive "skip frequency" parameter [5,6]. The drive performs a ramp up and ramp down test on the system such that problem frequencies can be detected.

Any frequencies that exhibit problems are (due to torsional vibrations at critical speeds, noise etc.) programmed out of the operating frequency range of the drive, such that these frequencies are avoided during operation of the system. How the skip frequency functionality operates is explained via a case study in the following section.

4   Investigation into resonance damping via a VSD case study

Industrial equipment ranging from mechanical cranes to pumps will have mechanical resonance frequencies based on the mechanical loading of the application. These resonance frequencies are the frequencies at which vibration can rapidly damage such mechanical equipment. These resonance frequencies can be determined by having the VSD ramp through the operating range such that the critical frequencies are identified.

VSDs have multiple skip frequency parameters such that problematic frequencies where resonance occurs can be avoided [5,6]. Most drive manufacturers (i.e. Schneider Electric and Opti Drive) offer multiple skip frequency parameters to mitigate different resonance frequencies.

4.1   Skip frequency operation

The skip frequency parameters are used to set up a band of frequencies through which the drive output frequency may pass, but never stop in. This is used typically to prevent continuous operation close to any frequency at which mechanical resonances may occur. Such resonances may simply cause excessive acoustic noise or may, in some cases, cause mechanical stresses that can lead to mechanical failure [5].

An example of the skip frequency bandwidth allocation is shown in Figure 6. In this case the OptiDrive VSD is used as an example. This can be found in the Optidrive advanced user manual [5].
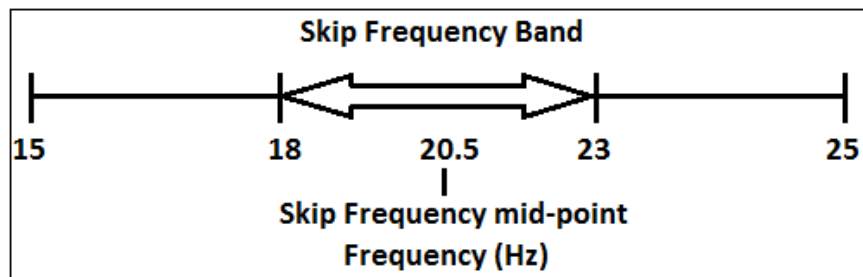

Figure 6: Skip frequency bandwidth allocation of an OptiDrive VSD [5].

When the resonance points are established from the ramp up and ramp down test of the mechanical load, the drive can then be programmed to "skip" these problem frequencies.

The skip frequency calculation is performed by the drive's internal software. The exact software algorithms are proprietary information and are not publicly available [7,8,9,10].

4.2   Skip frequency case study

A case study is investigated where a VSD is coupled with a fan that experienced torsional vibration effects during operation. The case study discusses the effects of the torsional vibrations on equipment and the remedy used to resolve the issue [11]. As will be discussed in a following section, there are many ways one can control a VSD. One of the most common and most basic is the constant Volts/Hertz control method. As torque control is not a major concern, the constant Volt/Hertz control is suitable for fan and pump applications [11]. When the drive is not correctly tuned to the motor, TNFs can be introduced into the system resulting in damaging vibrations to the equipment resulting in drive failure.

In this particular case study, the end user was experiencing reliability issues with an induced draft fan system after installing a VSD for control. With the VSD and motor in operation, the coupling between motor and induced draft fan had failed several times. As the motor had been coupled with the VSD for a relatively short time, the root cause of the problem was not yet fully understood. A short term solution at the time was to simply increase the coupling size between the motor and the shaft. Motor coupling sizes are defined by a Service Factor (SF), the higher the SF, the higher the torque rating of the coupling device [11]. This simply caused the problem to move to the next weakest link in the system, the motor shaft. With the change in the motor and shaft coupling, it was determined through further tests that the motor shaft would still fail due to torsional vibrations along the shaft. The damaged shaft is shown in Figure 7.
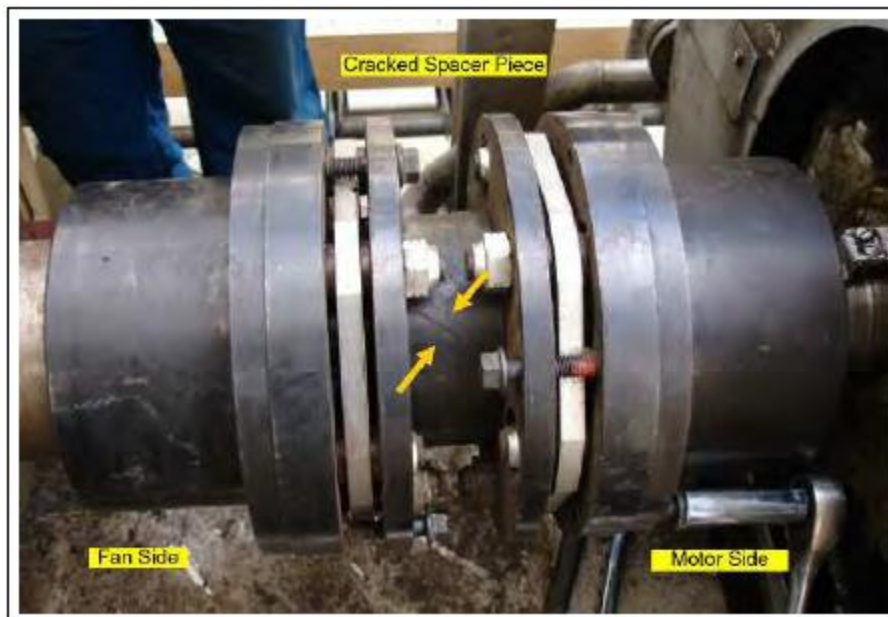
Figure 7: Cracked motor shaft as a result of torsional vibration [11].
Image from the 37th Turbomachinery Symposium used with publisher permission.

The 45 degree crack on the shaft shown in the photo is a classic indication of failure due to torsional vibrations [11]. In this case the coupling (which was already overrated when compared to previous failed couplings) on the drive was in service for less than a year when it failed and it was the third such coupling failure in a four year period.

A waterfall plot was done on the drive during startup. This plot is generated by stacking multiple frequency spectra in 10 rpm speed increments. During this startup procedure, a TNF was detected at 28.5 Hz. When passing through this torsional frequency, the dynamic torque would increase significantly which results in damaging dynamic torques being transmitted. A waterfall plot with the highlighted TNF occurring at 28.5 Hz is shown in Figure 8.
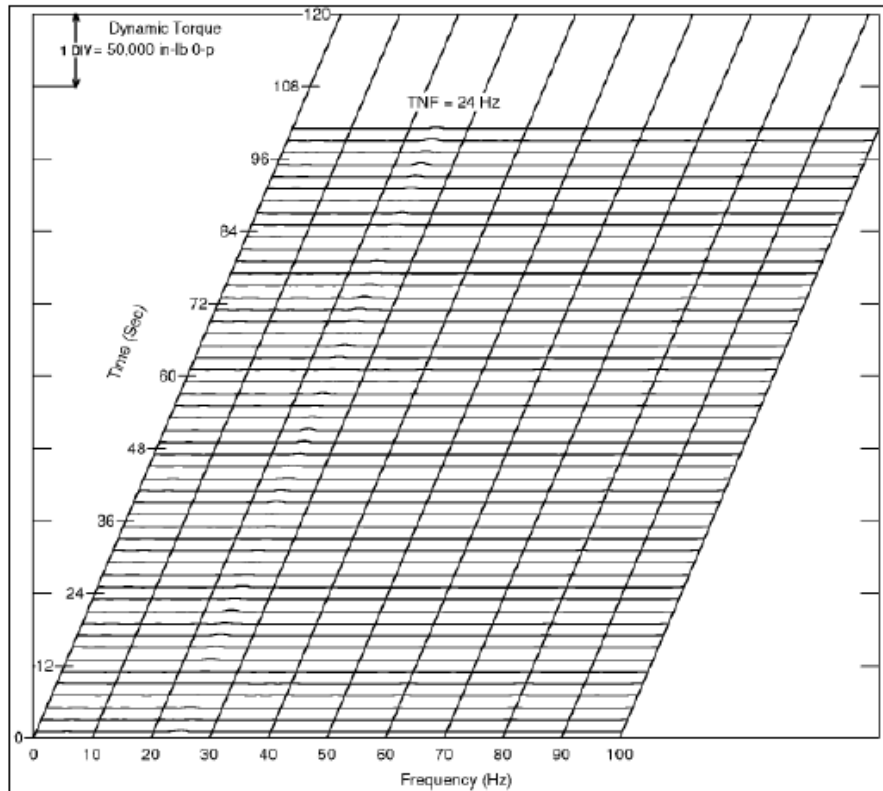
13
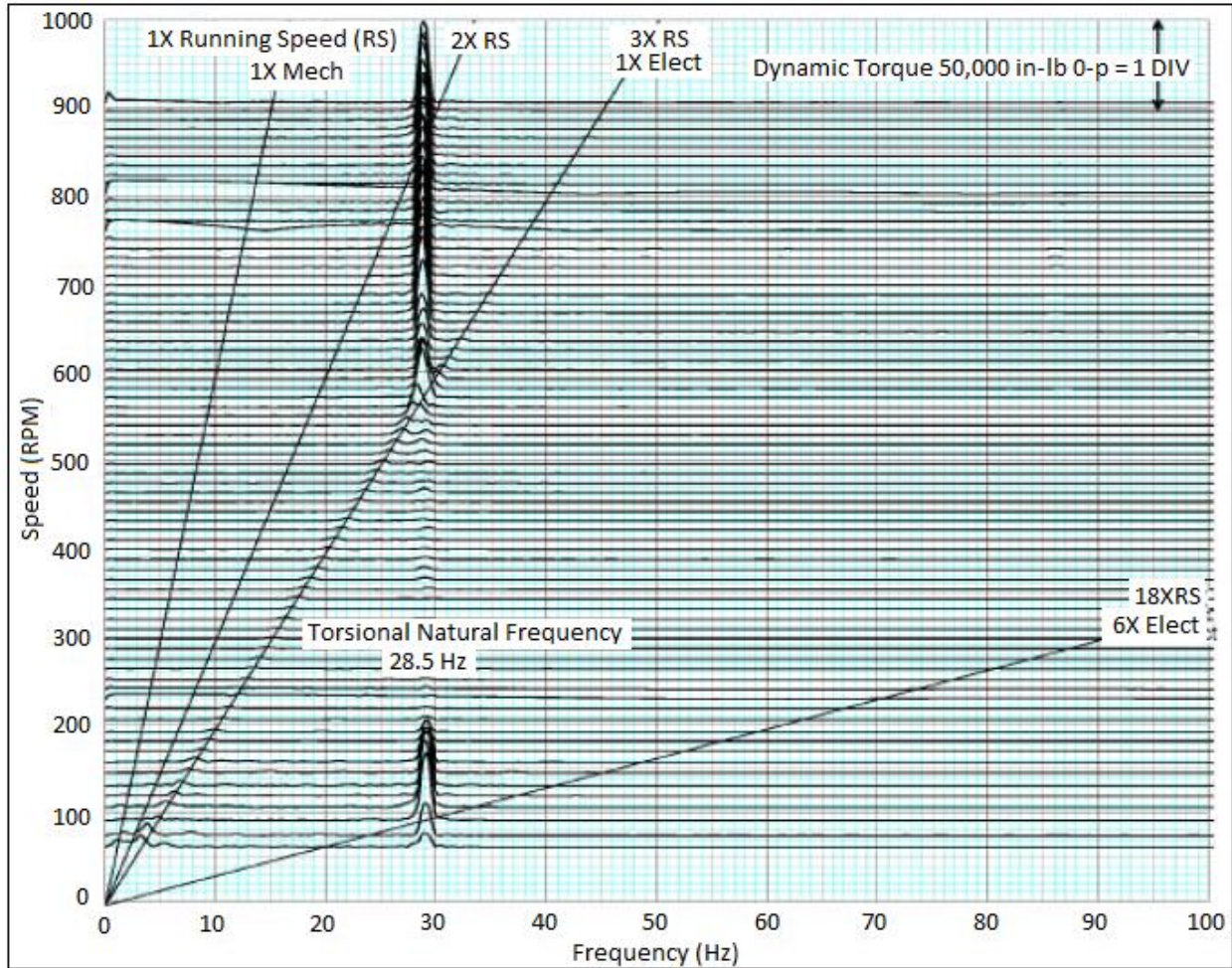
Figure 8: Waterfall plot with a torsional natural frequency shown [11].
Image from the 37th Turbomachinery Symposium used with publisher permission.

During the start-up sequence, it can be seen from the plot that the TNF was excited at 95 rpm and again later at 570 rpm. It was found that when passing through these torsional resonances the dynamic torque increased accordingly. Operation at, or around, this TNF would need to be avoided for normal operation of the drive. The drive parameters were adjusted to take into account the discovered TNF by setting the skip frequency to 29 Hz with a bandwidth of ±3 Hz.

With the drive re-configured, the problem was not entirely solved as the fan system would fail at a later stage with the same 45 degree crack in the shaft. With numerous drive settings attempted, the problem persisted and it was decided to run the VSD as a soft starter to determine if the drive was the cause of the TNF issue. A new coupling with the original specification was installed and it was found that the TNF would reduce to 24 Hz. This was attributed to the smaller coupling size and reduced overall torsional stiffness [11].

The VSD was then setup to operate in an "across-the-line" mode, also referred to as a bypass mode. In bypass mode, additional control circuitry is added such that the VSD is bypassed via an external contactor such that the VSD is then isolated from the load. When operating in this mode, it was found that the dynamic torque was greatly reduced. When operating the VSD in normal operation, the dynamic torque was dramatically increased. A waterfall plot of the drive running in "across-the-line" is shown in Figure 9.

Figure 9: Waterfall plot with VSD operating in "across-the-line" mode [11].
Image from the 37th Turbomachinery Symposium used with publisher permission.

From the new plot it can be seen that the TNF is now barely noticeable at 24 Hz. For this particular case, running the VSD in this manner was not a long term solution. The drive manufacturer was then contacted with the torsional model that was used and with the methods used to calculate the TNF based on the parameters of the motor and shaft from the installation. With the TNF calculation described earlier, the drive manufacturer was able to incorporate the torsional model into the electrical simulations of the drive. With the changes to the drive software, the following differences were noticed.

Table 4.2.1 : Comparison of old and new VSD drive configuration [11].

Item	Drive (with old software)	Drive (with updated software)
Duty Cycle update	1/carrier cycle	2/carrier cycle
Dead time Comp.	1/carrier cycle	2/carrier cycle
Bus voltage feedback	Non-linear filtering	Moving Average
DC Line choke	Saturating	Non-Saturating

Based on the new drive software, the dynamic torque still exceeded the safe operating limits at speeds noted at 560 rpm and 600 rpm (occurring at frequencies 26 Hz and 30 Hz respectively). In the analysis that followed, it was determined that when running through speeds of 700 rpm and 1200 rpm, the dynamic torque would reduce low enough that safe operation of the drive was possible.

For this particular case study, it was determined that the VSD was the source of much of the TNF experienced in the system. Discovering the VSD as the source of the excitation was determined when the drive was reconfigured as a soft starter. When bypassed the fan was operating at constant speed, when operating in this configuration the dynamic torque was reduced to 10% of the motor rated torque [11]. With new software installed in the drive and with the assistance of the drive manufacturer and setting the skip frequencies to 26 Hz and 30 Hz, the damaging torsional vibrations that would occur at those frequencies can be avoided.

The case study shows the effect torsional vibrations have on a mechanical shaft and system. In this study it was found that the VSD contributed to the problems in the system. In the simulation section of the research report, it will be assumed that the VSD will not interfere with the system. The case study serves as an example of what may occur in a real world configuration involving a VSD when compared to a VSD in a simulation environment.

The next section in the report will discuss the various control philosophies and will delve into the mathematical modeling of each. The modeling is presented such that whichever philosophy is used in a simulation, one has a basic understanding of what is occurring during the simulation.

5   Control topology for induction motors

DTC is a control technique used in VSDs to control the overall torque and speed of induction motors. DTC calculates the magnetic flux and torque based on measurements from the voltage and currents from the motor. A more detailed description will follow on the how DTC is achieved. There are various control philosophies that can be utilized. For the purposes of control of the motor, Space Vector Modulation (SVM) will be utilized with the DTC control scheme. A block diagram demonstrating the various control topologies is shown in Figure 10.
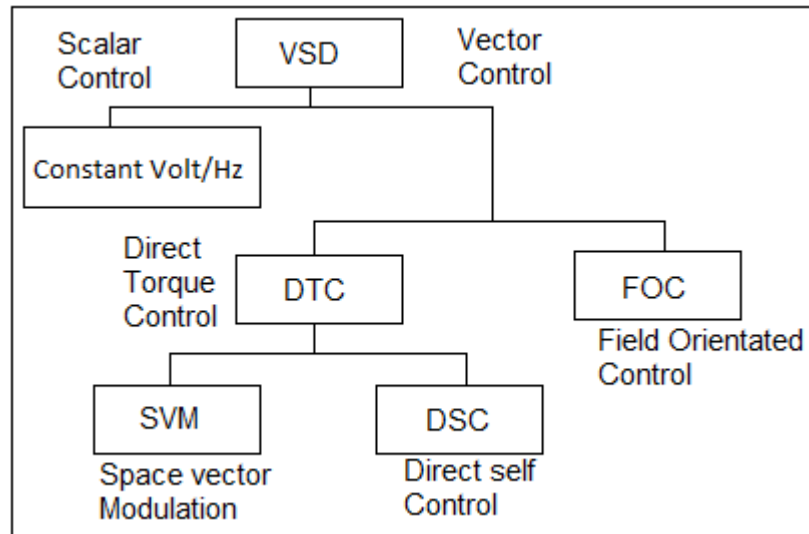

Figure 10: Various control topologies for a VSD.

In order to accurately describe what is occurring in the simulation, a description of the theory on what occurs via vector control, DTC and finally SVM will be discussed.

5.1   Dynamic analysis in terms of dq-windings

Before the simulation is analyzed, the equations to analyze the induction machine operation under dynamic conditions will be developed. Space vectors are used in transforming the a-b-c windings into the equivalent dq windings to obtain the stator and rotor transformation matrices.

While the motor is operating, the stator and flux linkages are dependent on the rotor angle [12]. In order to control an induction machine accurately using vector control, d- and q-axis analysis of the stator and rotor is required.

5.2   Stator *dq*-winding representation

A representation of the stator mmf by equivalent dq windings is shown in Figure 11.
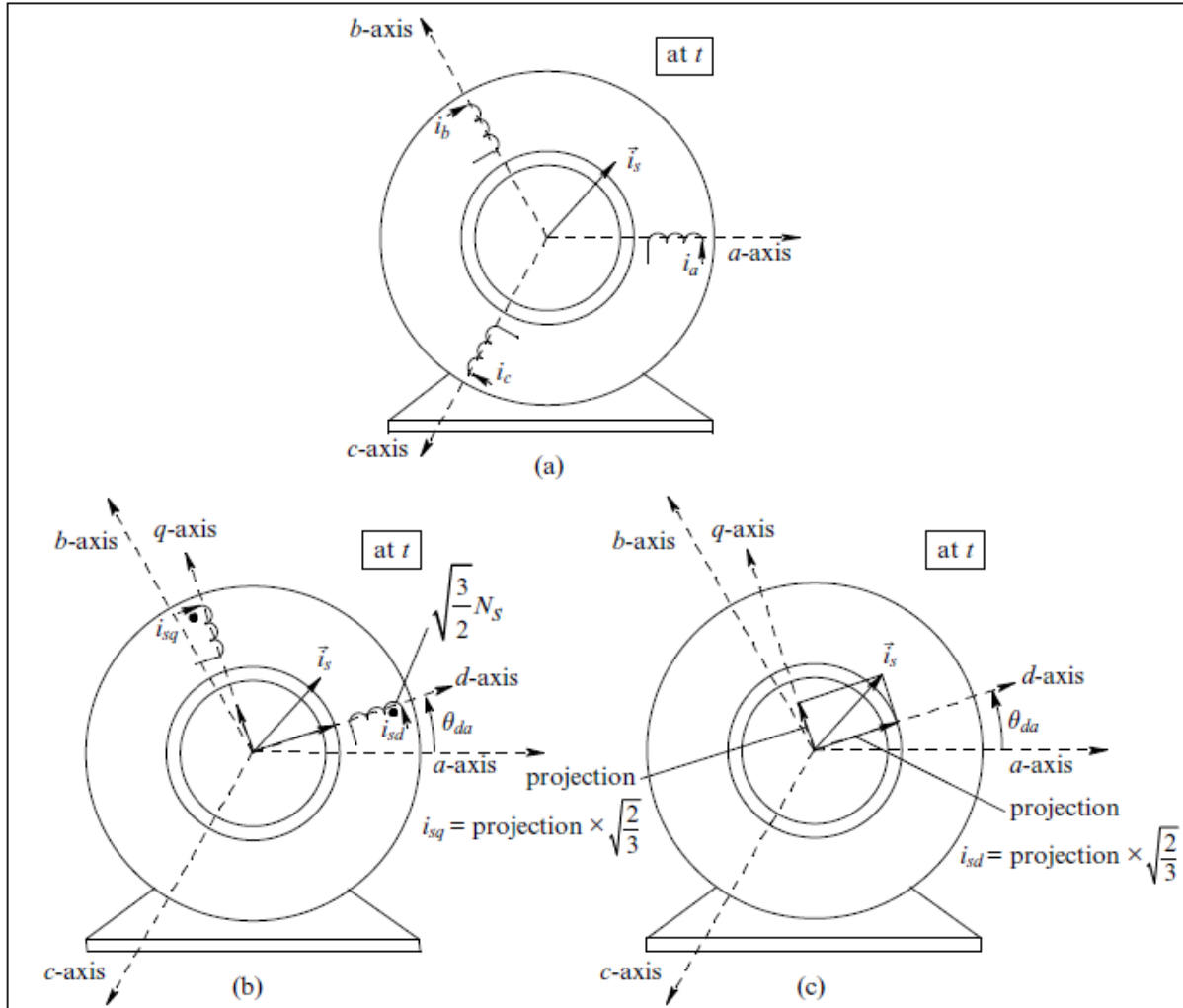

Figure 11: Representation of stator mmf by dq windings [12].
Image used with publisher permission.

At time t, the phase currents $i_a(t)$, $i_b(t)$ and $i_c(t)$ are represented by a stator current space vector $\vec{\imath_s}(t)$ An mmf space vector $\vec{F_s}(t)$ is related to the stator current space vector by a factor of $\frac{Ns}{p}$, with N_s being the number of turns per phase and p the number of poles. The stator current vector can be described as follows:

$$\vec{\imath_s^a}(t) = i_a(t) + i_b(t)e^{j2\pi/3} + i_c(t)e^{j4\pi/3} \tag{9}$$

For dynamic analysis and control of AC machines, two orthogonal windings must be synthesized such that the torque and the flux within the drive can be controlled independently [12].

At any one time, the air gap mmf distribution by three-phase windings can be produced by a set of two orthogonal windings (shown in Figure 11.b) with each being sinusiodally distributed by $\sqrt{\frac{3}{2}}$ N_s, one along the d-axis and the other along the q-axis. With this analysis the dq-windings are set to an angle θ_{da} with respect to the a-axis, the currents i_{sd} and i_{sq} in their respective windings will have specific values. These values can be obtained by equating the mmf produced by the dq windings that are produced by the three phase windings which can be represented by a single winding with turns N_s which is shown via the following equation [12].

$$\frac{\sqrt{3/2}.Ns}{p} \left(i_{sd} + ji_{sq}\right) = \frac{Ns}{p} \overrightarrow{\iota_s}^{d} \tag{10}$$

The stator current space vector is expressed using the d-axis as the reference axis and is shown as follows.

$$\left(i_{sd} + ji_{sq}\right) = \sqrt{\frac{2}{3}} \overrightarrow{\iota_s}^{d} \tag{11}$$

The above equation shows that the dq winding currents are $\sqrt{2/3}$ times the projection of the stator current space vector along the d- and q-axis. From Figure 11.c the i_{sd} and i_{sq} current vectors are $\sqrt{2/3}$ times the projection of the current space vector along the d and q axis respectively. Given this relationship the reciprocal factor of $\sqrt{3/2}$ is used in the number of turns for the dq-windings to ensure that the d and q winding currents produce the same mmf distribution as the three phase winding currents [12].

Figure 11.b shows that the d and q windings are mutually decoupled magnetically due to the orthogonal orientation. The $\sqrt{3/2}$ N_s turns for each winding causes the magnetizing inductance to be L_m. The magnetizing inductance is shown as follows.

$$L_m = \sqrt{\frac{3}{2}} \ L_{m,1-phase} \tag{12}$$

5.3   Rotor dq-winding representation

The rotor mmf space vector $\overrightarrow{F_r}$(t) is produced by the combined effect of the rotor bar, with bar having N_s turns. Figure 12 shows a representation of the rotor mmf by equivalent dq winding currents.
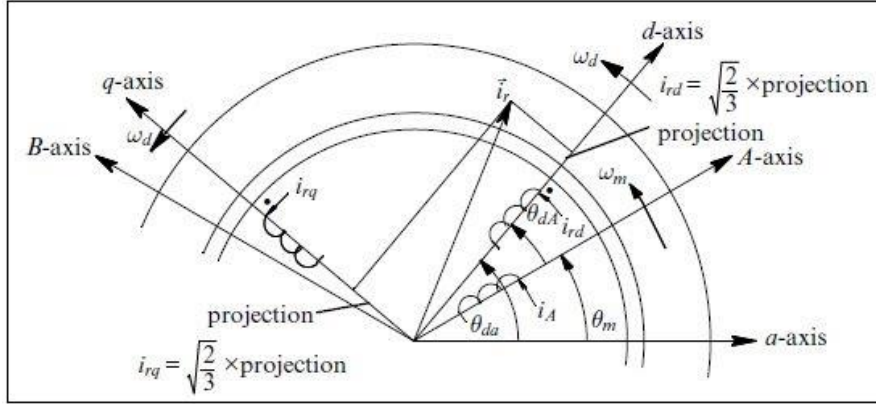
Figure 12: Representation of rotor mmf by dq windings [12].
Image used with publisher permission.

As with the stator current space vector, the rotor current space vector can be described as follows:

$$\vec{i}_r^A(t) = i_A(t) + i_B(t)e^{j2\pi/3} + i_C(t)e^{j4\pi/3} \tag{13}$$

The mmf and rotor current can be produced by the components i_{RD} and i_{RQ} flowing through their respective windings. It should be noted that the chosen d and q-axis for the rotor will be the same as the stator d and q-axis. The winding factor for the stator of $\sqrt{3/2} \cdot N_s$ will be the same for the rotor configuration, with the same magnetizing inductance, L_m due to both the stator and rotor having the same amount of turns [12].

Figure 13 demonstrates that by combining the dq stator and rotor windings one is able to obtain a stator and rotor representation by equivelant dq windings [12].

Figure 13: Stator and rotor representation by equivalent dq windings [12].
Image used with publisher permission.

The mutual inductance between the stator and rotor d-axis windings is equal to L_m. This is the result of the magnetizing flux crossing the air gap. The same mutual inductance value carries over to the q-axis as well.

5.4 Stator Mathematical relationship of the dq-windings

By equating the stator and rotor stator current vectors, one is able to determine the respective stator and rotor transformation matrices. From the stator and rotor representation of the equivalent windings, the d-axis from the stator perspective is shown to have an angle θ_{da} with respect to the a-axis. The stator current vector can be represented as follows:

$$\vec{\iota_s}(t) = \vec{\iota_s^a}(t)e^{-j\theta da(t)} \tag{14}$$

Substituting the equation (9) into equation (14) yields the following:

$$\vec{\iota_s}(t) = i_a e^{-j\theta da} + i_b e^{-j(\theta da - 2\pi/3)} + i_c e^{-j(\theta da - 4\pi/3)} \tag{15}$$

By equating the real and imaginary components to i_{sd} and i_{sq} the following transformation matrix to transform the stator a-b-c phase winding currents to the corresponding dq windings current known as $[T_s]_{abc->dq}$.

$$\begin{bmatrix} i_{sd}\ (t) \\ i_{sq}\ (t) \end{bmatrix} = \sqrt{\frac{2}{3}} \begin{bmatrix} \cos(\theta_{da}) & \cos(\theta_{da} - \frac{2\pi}{3}) & \cos(\theta_{da} - \frac{4\pi}{3}) \\ -\sin(\theta_{da}) & -\sin(\theta_{da} - \frac{2\pi}{3}) & -\sin(\theta_{da} - \frac{4\pi}{3}) \end{bmatrix} \begin{bmatrix} i_a\ (t) \\ i_b\ (t) \\ i_c\ (t) \end{bmatrix} \tag{16}$$

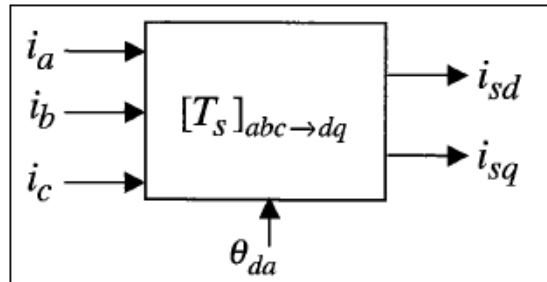A simple diagram explaining the transformation is showing Figure 14.

Figure 14: Block diagram of the stator transformation matrix [Ts]abc->dq [12].
Image used with publisher permission.

5.5 Rotor Mathematical relationship of the dq-windings

Similar steps are taken where the rotor phase currents are involved, as with the stator current vector. As before, from equation (7), the rotor current vector is represented as follows:

$$\vec{\iota_r^A}(t) = i_A(t) + i_B(t)e^{j2\pi/3} + i_C(t)e^{j4\pi/3} \tag{17}$$

As with the stator, from the rotor perspective, the d-axis is at an angle θ_{da}. The rotor current vector with respect to the A-axis is written as:

$$\vec{\imath_r}(t) = \vec{\imath_r}^A(t)e^{-j\theta dA(t)} \tag{18}$$

By applying the same substitution that was done with the stator, the following equation is obtained.

$$\vec{\imath_r}(t) = i_A e^{-j\theta dA} + i_B e^{-j(\theta dA - 2\pi/3)} + i_C e^{-j(\theta dA - 4\pi/3)} \tag{19}$$

Again by equating the real and imaginary components, the transformation matrix, $[T_r]_{ABC\text{->}dq}$ is obtained.

$$\begin{bmatrix} i_{rd}(t) \\ i_{rq}(t) \end{bmatrix} = \sqrt{\frac{2}{3}} \begin{bmatrix} \cos(\theta_{dA}) & \cos(\theta_{dA} - \frac{2\pi}{3}) & \cos(\theta_{dA} - \frac{4\pi}{3}) \\ -\sin(\theta_{dA}) & -\sin(\theta_{dA} - \frac{2\pi}{3}) & -\sin(\theta_{dA} - \frac{4\pi}{3}) \end{bmatrix} \begin{bmatrix} i_A(t) \\ i_B(t) \\ i_B(t) \end{bmatrix} \tag{20}$$

Similar with the stator block diagram, a block diagram representation is shown in Figure 15.
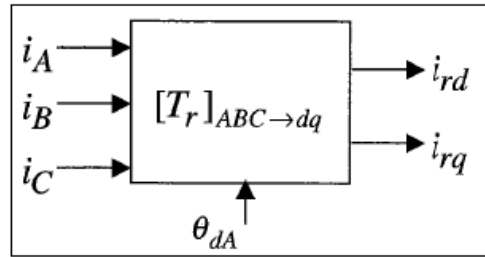
Figure 15: Block diagram of the rotor transformation matrix [Ts]ABC->dq [12].
Image used with publisher permission.

The inverse stator transformation matrix [T_s]_dq->ABC can be obtained via the following matrix.

$$\begin{bmatrix} i_a(t) \\ i_b(t) \\ i_c(t) \end{bmatrix} = \sqrt{\frac{2}{3}} \begin{bmatrix} \cos(\theta_{da}) & -\sin(\theta_{da}) \\ \cos(\theta_{da} + \frac{4\pi}{3}) & -\sin(\theta_{da} + \frac{4\pi}{3}) \\ \cos(\theta_{da} + \frac{2\pi}{3}) & -\sin(\theta_{da} + \frac{2\pi}{3}) \end{bmatrix} \begin{bmatrix} i_{sd} \\ i_{sq} \end{bmatrix} \tag{21}$$

A similar inverse transformation matrix can be obtained for the rotor by replacing the θ_{da} component of the above matrix with a θ_{dA} component, such that the inverse rotor transformation matrix [T_r]_dq->ABC is shown as follows:

$$\begin{bmatrix} i_A(t) \\ i_B(t) \\ i_C(t) \end{bmatrix} = \sqrt{\frac{2}{3}} \begin{bmatrix} \cos(\theta_{dA}) & -\sin(\theta_{dA}) \\ \cos(\theta_{dA} + \frac{4\pi}{3}) & -\sin(\theta_{dA} + \frac{4\pi}{3}) \\ \cos(\theta_{dA} + \frac{2\pi}{3}) & -\sin(\theta_{dA} + \frac{2\pi}{3}) \end{bmatrix} \begin{bmatrix} i_{sd} \\ i_{sq} \end{bmatrix} \tag{22}$$

It is these matrices that are present in the simulation that play a role in the vector control component of the simulation.
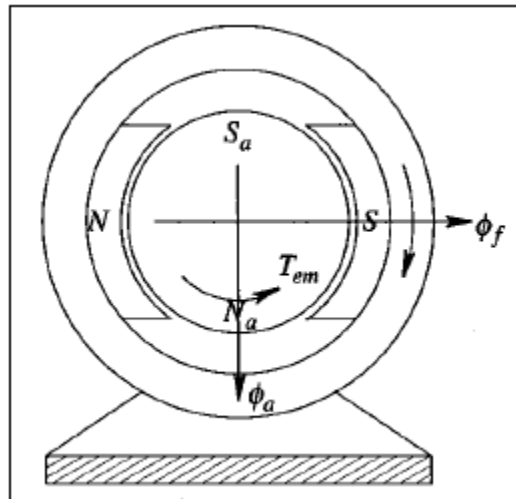
6   Vector control

In applications where accurate control of speed and position is required, vector control can be used. Vector control of an induction motor emulates the performance of a DC motor and brushless-DC motor servo drives [13]. In these applications torque is the variable that requires the most control where speed and position are critical. This section discusses how a step change in torque is achieved by vector control and how it applies to the simulation.

For a DC drive, the commutator and brushes ensure that the mmf produced by the armature-current is perpendicular to the flux produced by the stator field. With these fields remaining stationary, the electromagnetic torque T_{em} produced by the motor depends on a linear relationship with the armature current, $i_a,$ such that the torque equation is as follows:

$$T_{em} = k_T \cdot i_a \tag{23}$$

With the k_T component being the DC motor torque constant. In order to change T_{em} as a step, the armature current is changed as a step. In terms of an AC drive, this step change is done using a current controller. The current controller keeps the stator current space vector, $\vec{\iota_s}(t)$, 90 degrees ahead of the rotor field vector $\vec{B_r}(t)$, this is shown in Figure 16.

Figure 16: Example of control unit assistance, the stator current is 90° ahead of rotor field [13].
Image used with publisher permission.

Based on the stator current space vector being 90 degrees ahead of the rotor field vector, the torque T_{em}, depends on the amplitude of the stator current space vector $\hat{I}_s$.

The controller changes the amplitude of $\hat{I}_s$ to produce a step change in the torque. This is achieved be changing $i_a(t)$, $i_b(t)$, and $i_c(t)$ accordingly such that $\overrightarrow{i_s}(t)$, is kept 90 degrees ahead of $\overrightarrow{B_r}(t)$ in the direction of rotation [13]. A general layout of the controller that controls the current space vector and how it applies to the simulation is shown in Figure 17.
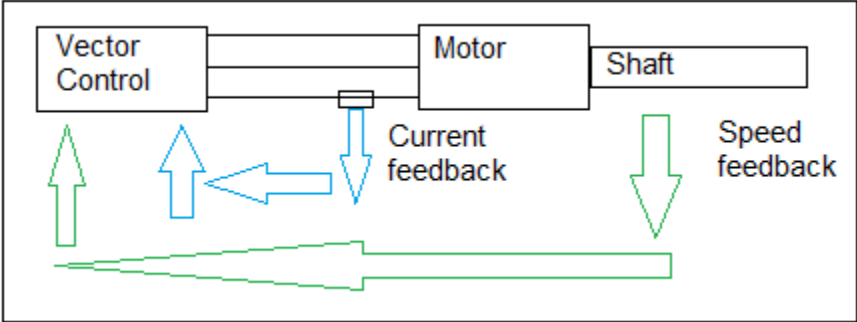

Figure 17: Basic vector control of the drive [13].

The overall task is to supply the desired currents based on the reference signals to the drive.

One method of achieving the currents required is in the use of hysteresis control [13]. The phase current is measured and compared with a reference value in the hysteresis comparator, the output of the comparator determines the switching state. An approximate waveform of the hysteresis control is shown in Figure 18.
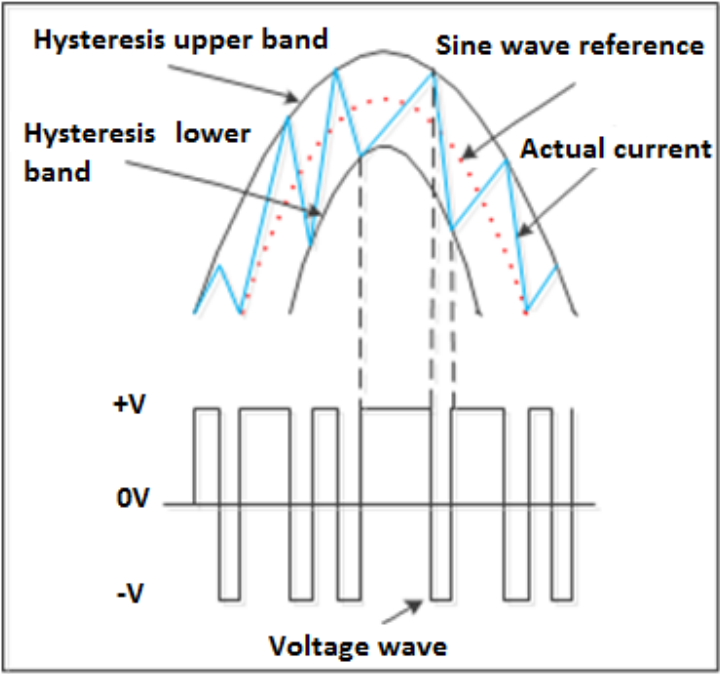
Figure 18: Approximate wave form via hysteresis control [14].

24

7   Direct Torque Control

The principle of DTC is to directly select voltage vectors according to the difference between reference and actual value of torque and flux linkage. If either the actual flux or torque deviates from the reference value more than the allowed tolerance, the DTC algorithm will control the VSD in such a manner that the actual flux and torque will return within their hysteresis band as fast as possible [15].

Depending on the position in the hysteresis band, a voltage vector is selected from a lookup table. This technique is referred to as Space Vector Modulation, which will be discussed in a later section. Advantages of DTC include a low level of complexity as that it requires only one motor parameter, the stator resistance. This resistance uses an Alpha (α) and Beta (β) reference frame for the stator when compared to the d and q references of the rotor and stator of vector control.

With DTC, one of six voltage vectors is applied during the sampling period and all calculations are done in a stationary reference frame [15]. A general block diagram of the DTC algorithm is shown in Figure 19.
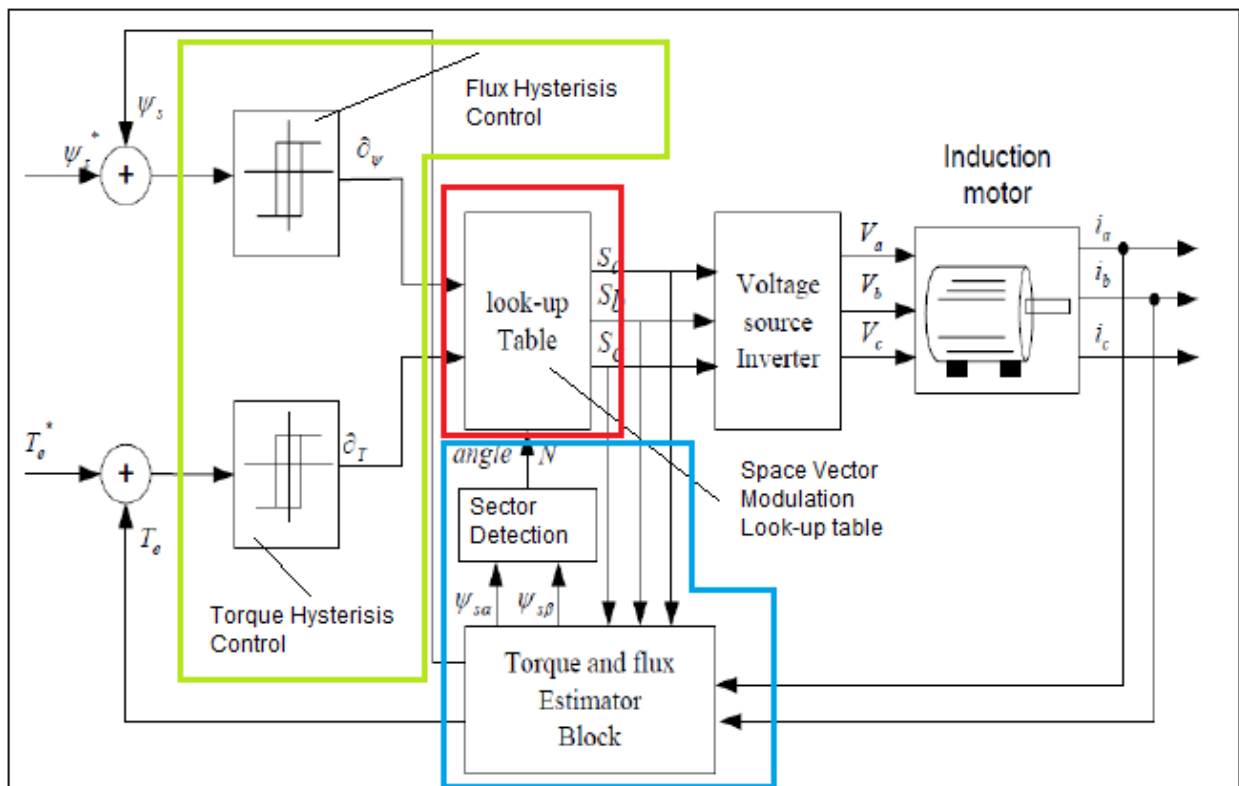
Figure 19: Block diagram of the DTC algorithm [15].
Image used with publisher permission, Copyright © 2012, IEEE.

From the above diagram, the green area indicates the flux hysteresis control, the blue is the torque and flux calculation and finally, the red is the SVM look-up table. As indicated, DTC aims to control the flux linkages directly rather than controlling the currents as is done in vector control. Within the Simulink model, a DTC control section gathers the torque and flux as inputs and feeds them into the DTC control model for calculation. The manner in which DTC control applies to the simulation, is shown in Figure 20.
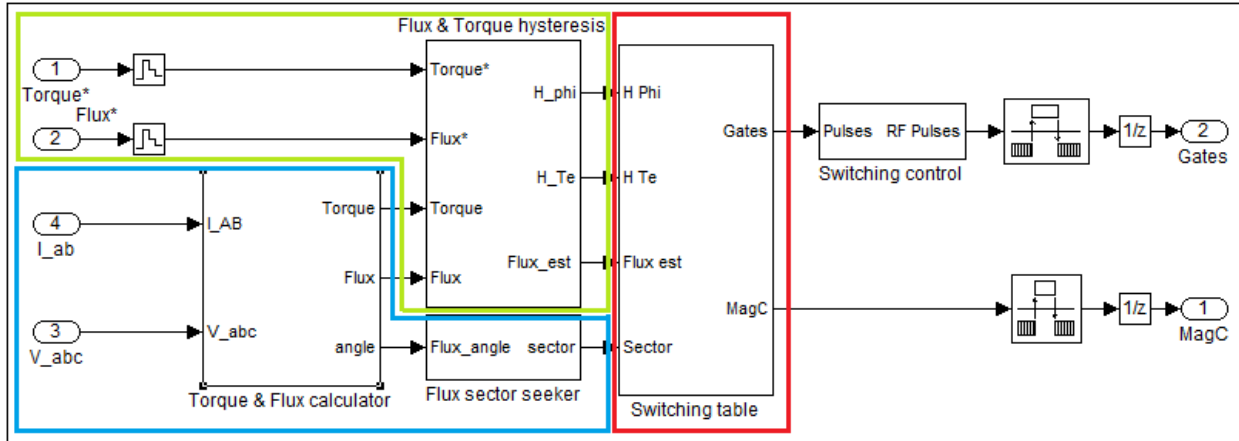
Figure 20: DTC block diagram from simulation.

7.1   Flux and Torque Hysteresis

The flux and torque hysteresis block contains a hysteresis comparator for the flux control and a hysteresis comparator for the torque control. For the torque hysteresis band, the value is the total band distributed symmetrically around the torque set point. For the stator flux hysteresis band, the value is the total band distributed symmetrically around the flux set point. Figure 21 show the hysteresis limit bands for the torque and hysteresis bands.
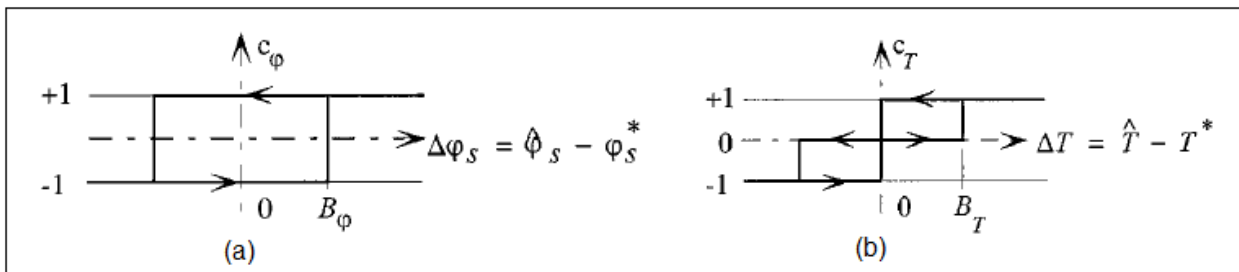
Figure 21: Flux (a) and Torque (b) comparator band limits [17].
Image used with publisher permission, Copyright © 2000, IEEE.

26

7.2   Flux and Torque Calculator and sector seeker

The torque and flux calculator control block is used to estimate the motor flux α and β components in addition to the electromagnetic torque component. The α and β control block is used to determine the sector of the α and β plane in which the flux vector lies. The α and β plane is divided into six different sectors spaced 60 degrees apart.

The eight vectors are referred to as the basic space vectors and are denoted by (V_0, V_1, V_2, V_3, V_4, V_5, V_6, V_7). Figure 22 shows the basic vector representation.
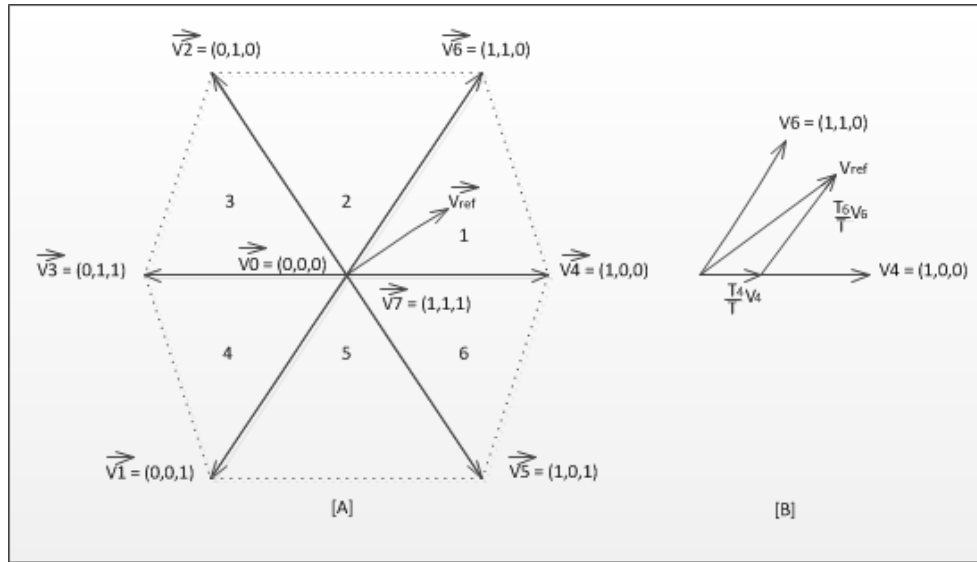
Figure 22: Basic voltage vectors (A) and the Sector 1 voltage vector (B) [18].

7.3   Switching table

The switching table block contains the lookup table that selects a specific voltage vector to correspond with the output of the flux and torque hysteresis comparators. This block is also used to produce the flux in the machine. The switching table is tabulated below.

Table 7.3.1: Look up table based on the voltage vectors [15].

Voltage Vectors	Switch Vectors			Line to Neutral Voltage			Line to Line Voltage		
	A	**B**	**C**	V_{an}	V_{bn}	V_{cn}	V_{ab}	V_{bc}	V_0
V_0	0	0	0	0	0	0	0	0	0
V_4	1	0	0	2/3	-1/3	-1/3	1	0	-1
V_6	1	1	0	1/3	1/3	-2/3	0	1	-1
V_2	0	1	0	-1/3	2/3	-1/3	-1	1	0
V_3	0	1	1	-2/3	1/3	1/3	-1	0	1
V_1	0	0	1	-1/3	1/3	2/3	0	-1	1
V_5	1	0	1	1/3	-2/3	1/3	1	-1	0
V_7	1	1	1	0	0	0	0	0	0

8   Space Vector Modulation

Space Vector Modulation (SVM) was developed as a vector approach to PWM for three phase inverters [15]. It is a more complicated method for generating a more sinusoidal output voltage that is then applied to the motor. The goal of any modulation technique is to obtain a variable output voltage with variable frequency having a maximum fundamental component with minimum harmonics [15]. Space Vector PWM (SVPWM) is an advanced method and possibly the best technique for variable frequency drive application.

In this modulation technique the three phase quantities can be transformed to their equivalent two-phase quantities either in a synchronously rotating frame or a stationary frame. From these two-phase components, the reference vector magnitude can be found and used for modulating the inverter output. When a three-phase voltage is applied to the AC machine it produces a rotating flux in the air gap of the AC machine. This rotating resultant flux can be represented as a single rotating voltage vector.

The magnitude and angle of the rotating vector is found by means of Clarke's Transformation [15]. To implement the SVPWM, the voltage in the stationary dq reference frame that consists of the horizontal (d) and vertical (q) axes is used, similar to that of Figure 12, for the dq windings with reference to the stator.

Based on the instantaneous current and voltage measurements, one can calculate the voltage required to drive the output torque current component and the stator flux current component to the required values. The required voltage is produced utilizing SVM. The voltage and motor currents can be used to estimate the instantaneous stator flux and output torque [15].

If the inverter is not capable of generating the required voltage then the voltage vector which will drive the torque and flux towards the demand value is chosen and held for the complete cycle.

With the various modulation techniques for multilevel inverters, SVPWM has a number of advantages. Firstly, it directly uses the control variable given by the control system and identifies each switching vector as a point in complex (α, β) space. Secondly, it is suitable for digital signal processor implementation and finally, it can optimize switching sequences [15]. From the basic vector diagram shown in Figure 22, SVPWM is able to split the vectors into further regions by splitting each sector into triangles as shown in Figure 23.
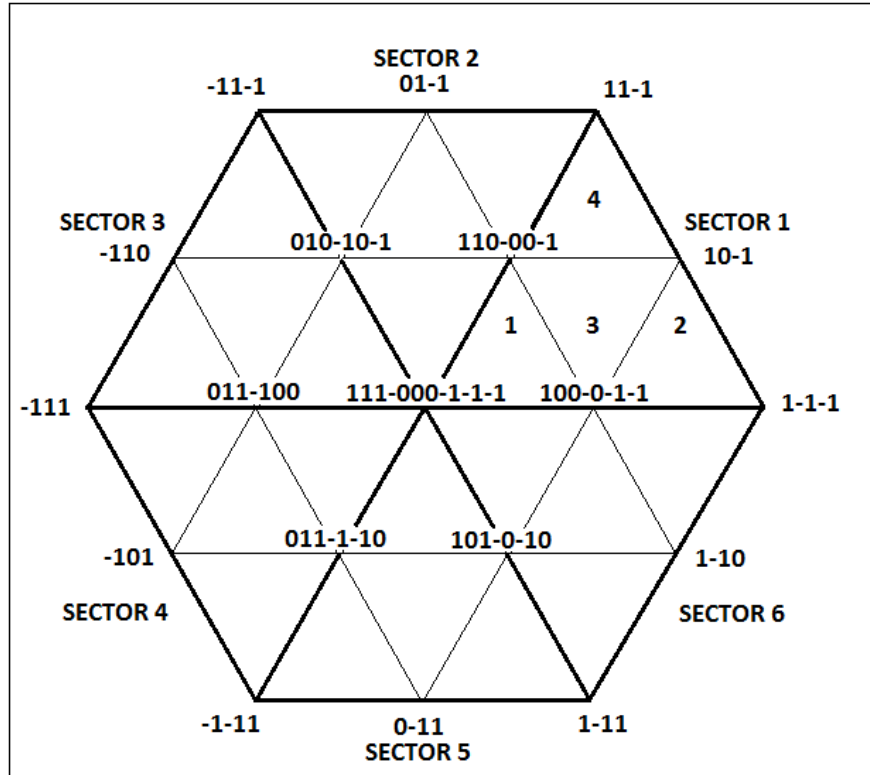
Figure 23: Space Vector diagram of a three-level inverter [16].

9   Electrical and mechanical circuit modeling

In order to discuss how a torque damping effect occurs in a rotational system, two systems will be analyzed via first principles. The analyses of the two systems will then be used to develop a third system of a rotational torsional system. The first system will be that of an RLC electrical circuit and the second system will describe the mechanical analogue to the RLC electrical circuit via a mechanical spring-damper system and how damping is achieved in these systems.

The third system will be that of a rotational mechanical system with its elements translated from the spring-mass-damper mechanical system. Before the damping effect can be described, a simple LC circuit will be analyzed with oscillating behavior and how introducing a resistor can provide a damping effect. Upon the completion of the rotational mechanical analogue, the rotational model will then be applied to a wind turbine system and a VSD acting as a resistor can provide damping following a disturbance in the system.

9.1   Oscillations in an LC circuit

When an inductor is connected to a capacitor, they form a simple LC circuit as shown in Figure 24.
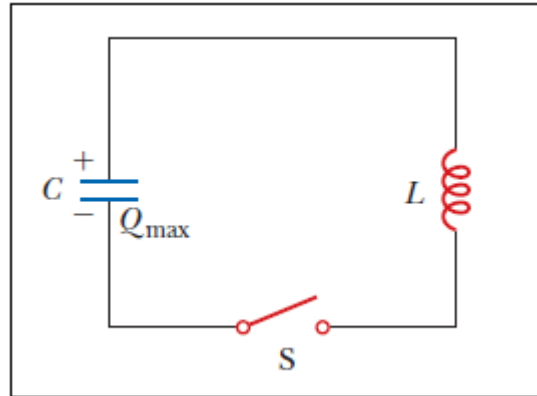
Figure 24: Simple LC circuit [19].
Image used with publisher permission.

If the capacitor is assumed to be initially charged when the switch is closed, both the current in the circuit and the charge on the capacitor will oscillate between maximum positive and negative values [19]. If the resistance in the circuit is assumed to be zero, no energy is dissipated. With zero resistance, the oscillations in the circuit will persist indefinitely.

Observing the circuit from an energy standpoint, it will be assumed that the capacitor has an initial charge Q_{max} and the switch is thrown $t = 0$. The energy U in the circuit is stored in the electric field of the capacitor and is equal to $\frac{Q_{max}^2}{2C}$. At this moment, the current in the circuit is zero and no energy is stored in the inductor. After the switch is closed, the rate at which charge leaves or enters the capacitor is equal to the current in the circuit. When the switch is closed, the capacitor begins to discharge and the energy in its electric field decreases. The discharging effect of the capacitor now represents a current in the circuit and some energy is stored in the magnetic field of the inductor [19]. Energy is transferred from the electric field of the capacitor to the magnetic field of the inductor.

When the capacitor is fully discharged, it will store no energy. At this moment, the current reaches its maximum value and all of the energy is stored in the inductor. The current will continue in the same direction, decreasing in magnitude, with the capacitor becoming fully charged, with the opposite voltage polarity. This is then followed by another discharge until the circuit returns to its original state of charge, Q_{max} with plate polarity that was shown in Figure 24. The energy continues to oscillate between the inductor and the capacitor [19].

The oscillations of the LC circuit are an electromagnetic analog to the mechanical oscillations of a mass-spring system. A graphical representation of the energy transfer of the LC circuit and that of a mechanical spring-mass equivalent system is shown in Figure 25.
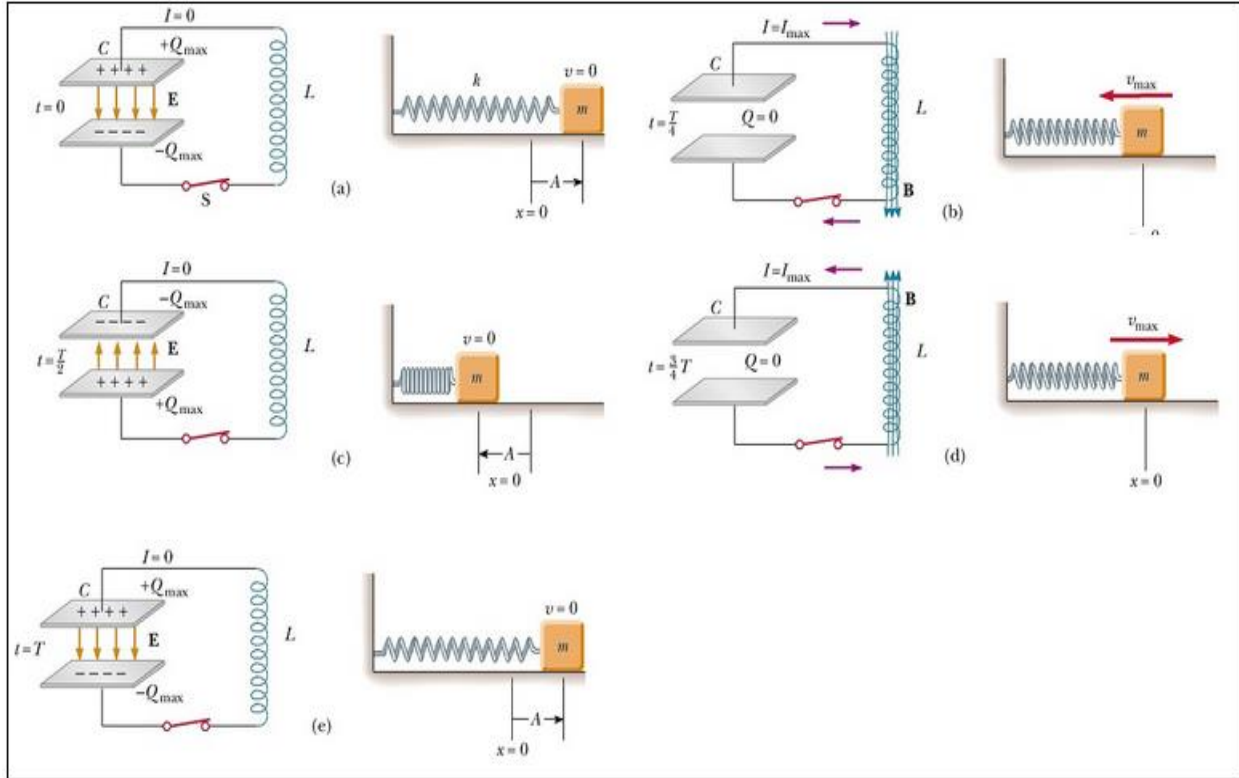
Figure 25: Energy transfer in an LC circuit and equivalent spring-mass mechanical analog [19]. Image used with publisher permission.

It can be noted from Figure 25, with assuming a maximum charge on the capacitor, Q_{max}, at $t = 0$ the mass is positioned in an equivalent position such that the spring is fully extended.

For the above figure, the intervals are shown in one-fourth the period of oscillation T. The potential energy $\frac{1}{2}kx^2$ stored in a stretched spring is analogous to the electrical potential energy $\frac{Q_{max}^2}{2C}$ stored in the capacitor [19]. The kinetic energy, $\frac{1}{2}mv^2$, of the moving block is analogous to the magnetic energy, $\frac{1}{2}LI^2$, stored in the inductor. In Figure 25-(a), all the energy is stored as electric potential energy in the capacitor at $t = 0$. In Figure 25-(b), where t is one-fourth that of the period T, all the energy is stored as magnetic energy, $\frac{1}{2}LI^2{}_{max,}$ in the inductor, where I_{max} is the maximum current in the circuit. Figure 25-(c) shows the energy in the circuit is now completely stored in the capacitor, with the polarity of the plates in now in the opposite direction when compared to plates at $t = 0$.

Considering an arbitrary time t after the switch is closed, such that the capacitor has a charge $Q < Q_{max}$ and current is $I < I_{max}$.

During this time, both LC elements will store energy and the sum of the energies must equal the total initial energy U stored in the fully charged capacitor at $t = 0$. The equation the total energy in the system is represented as follows:

$$U = U_c + U_L = \frac{Q^2}{2C} + \frac{1}{2}LI^2 \tag{24}$$

In the initial assumption, the circuit resistance is assumed to be zero, such that no energy is dissipated. Under this assumption, the total energy must remain constant in time, indicating that $\frac{dU}{dt} = 0$. Differentiating the above equation with respect to time, with Q and I varying with time, the following equation is obtained [19].

$$\frac{dU}{dt} = \frac{d}{dt}\left(\frac{Q^2}{2C} + \frac{1}{2}LI^2\right) = \frac{Q}{C}\frac{dQ}{dt} + LI\frac{dI}{dt} = 0 \tag{25}$$

The equation can be simplified further if one takes into account that the current in the circuit is equal to the rate at which the charge on the capacitor changes, designated by $I = \frac{dq}{dt}$. This results in Equation 25 taking the form of as follows:

$$\frac{Q}{C} + L\frac{d^2Q}{dt^2} = 0 \tag{26}$$

Solving for $\frac{d^2Q}{dt^2}$ results in the following:

$$\frac{d^2Q}{dt^2} = -\frac{Q}{LC} \tag{27}$$

It can be noted that the above expression takes the same form as the analogous spring-mass equations as follows:

$$\frac{d^2x}{dt^2} = -\frac{k}{m}x = -\omega^2 x \tag{28}$$

Where k is the spring constant, m is the mass of the block and $\omega = \sqrt{k/m}$. The equation then has the general form of:

$$x = A\cos(\omega t + \phi) \tag{29}$$

Where ω is the angular frequency of the simple harmonic motion, A is the amplitude of motion (the maximum value of x) and ϕ is the phase constant. Such that the charge equation can take the following form:

$$Q = Q_{max}\cos(\omega t + \phi) \tag{30}$$

The term Q_{max} in the above equation is the maximum charge of the capacitor and the angular frequency is represented by:

$$\omega = \frac{1}{\sqrt{LC}} \tag{31}$$

From the above equation, it can be noted that the angular frequency of the oscillation is a function of the inductance and capacitance. This is referred to as the natural frequency of oscillation of the LC circuit [19].

As the charge, Q, varies sinusoidally, so will the current, I, also vary sinusodally in the circuit. This can be shown by differentiating equation 30 with respect to time and obtaining the following equation:

$$I = \frac{dQ}{dt} = -\omega Q_{max} \sin(\omega t + \phi) \tag{32}$$

In order to determine the phase angle, ϕ, one is required to set initial conditions at $t = 0, I = 0$ and $Q = Q_{max}$. Equation 32 now becomes the following:

$$0 = -\omega Q_{max} \sin(\phi) \tag{33}$$

With the initial conditions, the phase angle is zero. The phase angle is consistent with Equation 30. With the condition that $Q = Q_{max}$ at setting $t = 0$, the follow equations for Q and I are obtained [19].

$$Q = Q_{max} \cos(\omega t) \tag{34}$$

$$I = -\omega Q_{max} \sin(\omega t) \tag{35}$$

$$= -I_{max} \sin(\omega t)$$

The graphical representation of Q versus t and I versus t is shown in Figure 26.
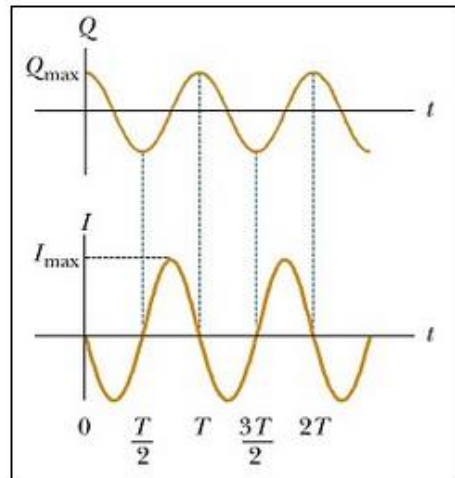
Figure 26: Charge and Current versus time [19].
Image used with publisher permission.

From Figure 26 it can be noted that the charge on the capacitor oscillates between extreme values of Q_{max} and $-Q_{max}$ with the current oscillating between I_{max} and $-I_{max}$. It can also be seen that the current is 90 degrees out of phase with the charge. Such that when the charge is at its maximum, the current will be zero and when the charge is zero, the current will be at its maximum value [19].

33

In the LC circuit analyses, it was noted that with no circuit resistance, the oscillation will continue indefinitely. Realistically, with circuit resistance and a capacitor's equivalent series resistance (ESR), with ESR being defined as losses from a capacitor due to the resistance of the dielectric plates, energy will be dissipated in the circuit. This then leads to an analysis of an RLC circuit.

9.2 The RLC circuit and mass-spring-damper system

Taking the LC circuit and adding a resistor in series with the inductor and capacitor circuit results in the circuit shown in Figure 27.
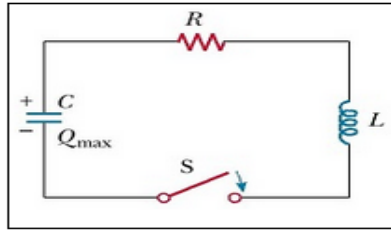
Figure 27: Series RLC circuit [19].
Image used with publisher permission.

As before, the capacitor is assumed to have an initial charge of Q_{max} at $t = 0$ when the switch is closed. As previously, the energy at any given time is given by Equation 24. However with this circuit configuration, the energy is no longer constant as was with the LC circuit, as the resistor now dissipates energy. As the rate of dissipation of energy from the resistor is given by I^2R, the following equation is obtained. Ideally, a lossless capacitor is assumed, with an ESR of zero.

$$\frac{dU}{dt} = -I^2R \tag{36}$$

The negative sign in the equation indicates the energy is decreasing in time. Substituting this component into equation 26 gives the following equation:

$$\frac{Q}{C}\frac{dQ}{dt} + LI\frac{dI}{dt} = -I^2R \tag{37}$$

In order to convert the equation into an electrical equation that compares electrical oscillations to that of a mechanical analog, we use the form from Equation 32, that $I = \frac{dQ}{dt}$ and substitute into the above equation and shift the terms to the left-hand side and divide through by I to give the following equation for the RLC circuit:

$$L\frac{d^2Q}{dt^2} + R\frac{dQ}{dt} + \frac{Q}{C} = 0 \tag{38}$$

The RLC circuit equation is now analogous with a damped mechanical oscillator circuit equation shown as follows:

$$m\frac{d^2x}{dt^2} + b\frac{dx}{dt} + kx = 0 \tag{39}$$

Observing the equivalent mechanical circuit for Figure 25 and using the above equation, the following analogous system to that of the RLC circuit if shown in Figure 28.

Figure 28: Block-spring system analogous to a RLC circuit [19].
Image used with publisher permission.

In Figure 28, the resistive component of the mechanical analogue is represented by a viscous medium. The damped harmonic motion is representative of the RLC circuit. When observed from a Force-Current viewpoint, it can be noted that displacement, x, corresponds to flux linkage, ψ. The reciprocal of inductance, L, corresponds to spring stiffness, k, while the capacitance, C, corresponds to m, the mass of the block. How these terms relate to a rotational mechanical system in terms of velocity and torque will be discussed in the section that follows on from this discussion, in the rotational mechanical system analysis.

If we assume the value of the resistance in the RLC circuit to be small (a situation that would provide a light damping effect in the mechanical analogue) the following equation is obtained:

$$Q = Q_{max} e^{\frac{-Rt}{2L}} \cos(\omega_d t) \tag{40}$$

The ω_d term is representative of the following:

$$\omega_d = \sqrt{\frac{1}{LC} - \left[\frac{R}{2L}\right]^2} \tag{41}$$

This equation represents the angular frequency at which the circuit oscillates. This indicates the charge on the capacitor experiences a damped harmonic oscillation which is analogous to the mass-spring system in the viscous liquid shown in Figure 28.

A figure showing a side by side comparison of the charge versus time of the LC circuit (with no resistance assumed) when compared to that of the RLC charge versus time circuit is shown in Figure 29.
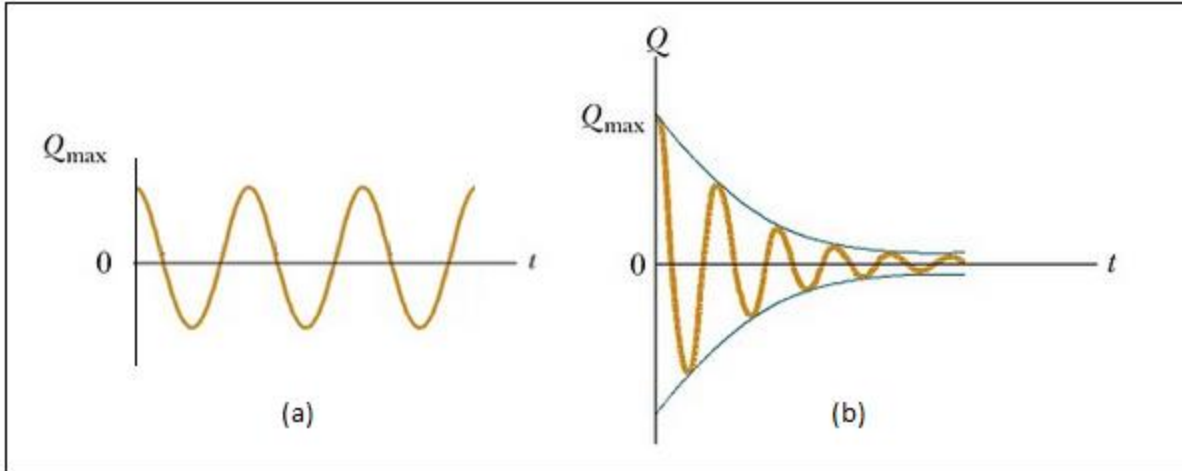
Figure 29: LC circuit (a) versus RLC circuit (b) charge versus time [19].
Image used with publisher permission.

From Figure 29, it can seem that the maximum value of Q_{max} decreases with each oscillation, just as the amplitude of displacement of the damped block-spring would damp over time. As the current, $I = \frac{dQ}{dt}$ it can be observed that the current undergoes a damped oscillation behavior in the RLC circuit. With the RLC circuit and its resistive component defined, the equivalent spring-mass-damper mechanical analogue would take the following form shown in Figure 30.
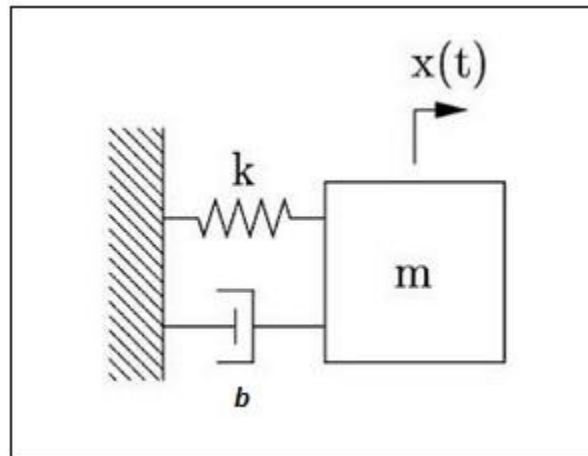
Figure 30: Spring-mass-damper mechanical analogue to a RLC circuit.

With the electrical and mechanical systems modeled, the analogies of the RLC electrical circuit and the mechanical system can be summarized via the table below using force-current and velocity-voltage analogies.

Table 9.2.1: Force-current and velocity-voltage analogies between electrical circuits and mechanical translational motion systems [19].

Electric circuit		Mechanical translational motion system
Voltage	$v \leftrightarrow m/s$	Velocity
Current	$i \leftrightarrow f$	Force
Flux linkage	$\psi \leftrightarrow x$	Displacement
Capacitance	$C \leftrightarrow m$	mass
Reciprocal of Inductance	$\frac{1}{L} \leftrightarrow k$	Torsional Spring stiffness
Reciprocal of Resistance	$\frac{1}{R} \leftrightarrow b$	Viscous friction coefficient
RLC Circuit	$C\frac{d^2\psi}{dt^2} + \frac{1}{R}\frac{d\psi}{dt} + \frac{1}{L}\psi = 0 \leftrightarrow$ $m\frac{d^2x}{dt^2} + b\frac{dx}{dt} + kx = 0$	Damped mass on a spring

9.3 The rotational motion mechanical system

Now that the electrical and translational mechanical systems have been covered to serve as a frame work, the rotational mechanical system is derived. Rotational mechanical systems are handled in the same manner as translational mechanical systems. Except that torque replaces force and angular displacement replaces translational displacement [20]. The mechanical components for the rotational system are the same with the exception that the components undergo rotation instead of translation.

The component with their relationships between torque, angular velocity and angular displacement are shown in Figure 31.
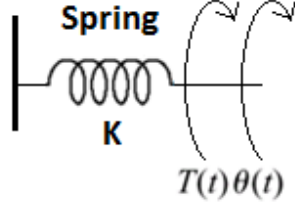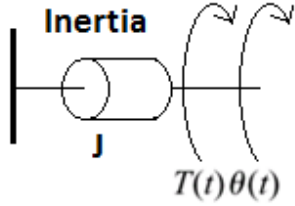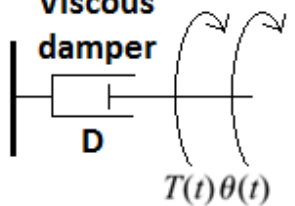
Component	Torque-angular velocity	Torque-angular displacement	Impedance $Z_M(s) = \dfrac{T(s)}{\theta(s)}$
Spring K $T(t)\theta(t)$	$T(t) = K\displaystyle\int_0^t \omega(\tau)\,d\tau$	$T(t) = K\theta(t)$	K
Inertia J $T(t)\theta(t)$	$T(t) = J\dfrac{d\omega(t)}{dt}$	$T(t) = J\dfrac{d^2\theta(t)}{dt^2}$	Js^2
Viscous damper D $T(t)\theta(t)$	$T(t) = D\omega(t)$	$T(t) = D\dfrac{d\theta(t)}{dt}$	Ds

Figure 31: Component relationships between torque, angular velocity and angular displacement [20].

From Figure 31, it can be noted that the symbols are the same as the translational mechanical system, but in this case, the components are undergoing rotation. The term associated with mass has been replaced with moment of inertia. The impedance terms K, D and J are referred to as the spring constant (expressed in N-m/rad), the coefficient of viscous friction (expressed in N-m-s/rad) and the moment of inertia (expressed in kg-m^2), respectively.

An example of how the components are applied to a rotating mechanical system is shown in Figure 32.
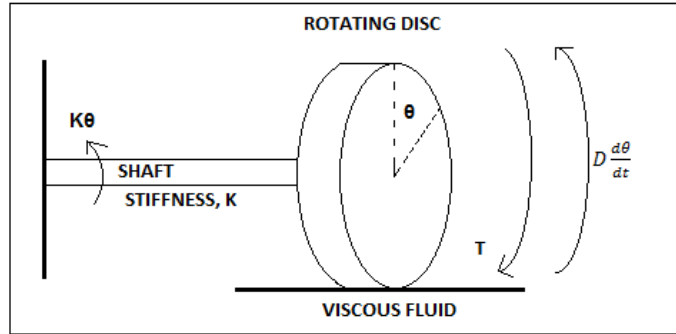
Figure 32: Rotating mechanical system [21].

The term T in the above figure is the torque that allows the disc to turn. The three basic components of the rotational system is the moment of inertia, the viscous friction and the torsional spring component. From Figure 31, the equation that governs the rotating mechanical system is as follows:

$$T = J\frac{d^2\theta}{dt^2} + D\frac{d\theta}{dt} + K\theta \tag{42}$$

For the above rotational mechanical system, the equivalent mechanical system is shown in Figure 33.
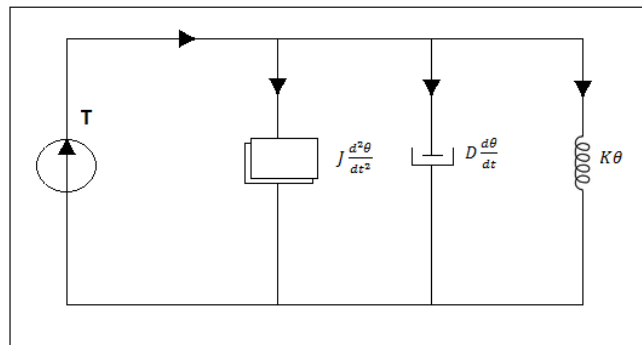
Figure 33: Mechanical equivalent of a rotational system [21].

The circuit shown in the figure above describes that of the torque-current and angular velocity-voltage analogies. Such that the equivalent RLC circuit for a torque-current and angular velocity-voltage analogous system is shown in Figure 34, it can noted that the torque in the system is now represented by current and is driven by a current source.
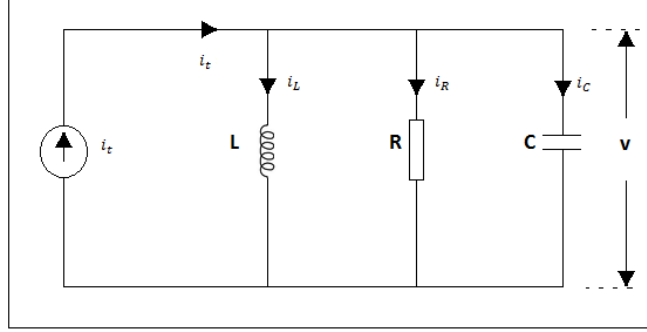
Figure 34: RLC equivalent circuit [21].

The figure above is analyzed with the following equations:

$$i_t = i_L + i_R + i_C \tag{43}$$

Such that for the capacitive element, the equation are as follows:

$$q = Cv = \int i_c dt$$

$$i_C = C \frac{dv}{dt} \tag{44}$$

For the inductive element, the equation is as follows:

$$i_L = \frac{1}{L} \int v \, dt \tag{45}$$

And finally, the resistive element is shown as follows:

$$I_R = \frac{v}{R} \tag{46}$$

Substituting the above equation into equation 43 gives the following equation:

$$i_t = \frac{1}{L} \int v \, dt + \frac{v}{R} + C \frac{dv}{dt} \tag{47}$$

In terms of flux linkages, ψ, equation 47 can be represented by substituting v with $\dfrac{d\psi}{dt}$ which results in the following equation:

$$i_t = C \frac{d^2\psi}{dt^2} + \frac{1}{R} \frac{d\psi}{dt} + \frac{1}{L} \psi \tag{48}$$

This equation can now be compared to the translational mechanical system from equation 39. With this equation, the torque-current and angular velocity-voltage analogies for a mechanical rotational motion system and electrical circuit are shown in the table below.

Table 9.3.1: Force-current and velocity-voltage analogies between mechanical translational motion systems, electrical circuits and torque-current and angular velocity-voltage analogies for a mechanical rotational motion system [21].

Mechanical translational motion systems	Electrical circuits	Mechanical rotational motion systems
Force, f	Current, i	Torque, T
mass, M	Capacitance, C	Moment of inertia, J
Viscous friction coefficient, D	Reciprocal of resistance, $1/R$	Viscous friction coefficient, D
Spring stiffness, k	Reciprocal of inductance, $1/L$	Torsional spring stiffness, K
Displacement, x	Flux linkage, ψ	Angular displacement, θ
Velocity, m/s	Voltage, v	Angular velocity, ω

Finally, from the above table, the equation that governs how a mechanical rotational system oscillates can be obtained. From equation 41, the resulting equation on the oscillation of a rotational system can be expressed as follows:

$$\omega = \sqrt{\frac{K}{J} - \left[\frac{D}{2J}\right]^2} \tag{49}$$

9.3.1 Disturbance damping in an electrical and mechanical system

Prior to analyzing the disturbance damping from an electrical and mechanical standpoint, the parameters of the RLC circuit in Figure 27 will be defined such that the behavior of the system can be observed when applying unit step input. In order for the voltage and current waveforms to be in-phase during a disturbance, the reactance of the inductor and capacitor are required to be equal, the inductive reactance is calculated with $X_L = 2\pi f L$, while the capacitive reactance is calculated with $X_C = 1/2\pi f C$. A frequency of 50 Hz will be used in both cases.

For the first case, the resistor value is set to 1 Ω, the inductor is set to 20 mH, and finally, the capacitor is set to 506.621 µF. Given these parameters, the reactance of the inductor and capacitor will have equal values of 6.283 Ω. A unit step input is applied and the system response is observed in Figure 35-(a).

For the second case, to achieve a scenario where the current waveform to lags the voltage, the inductive reactance is required to be increased. The resistor and capacitor values will remain unchanged. The inductor value is now set to 100 mH. This results in an inductive reactance value of 31.416 Ω. A unit step input is applied, and the system response is observed in Figure 35-(b).

With the electrical and mechanical analogue systems described, two waveforms will be analyzed via the RLC circuit and two waveforms from the mechanical system perspective. The first waveform will be that of the voltage and current waveforms being in-phase, leading to a critically damped response when a disturbance occurs. The same waveforms for speed variation and torque will be carried over to the mechanical system, describing how applying a torque in-phase with the speed variation provides a damping torque.

A second set of waveforms will describe the disturbance response when the voltage and current versus the speed variation and torque waveforms are applied slightly out-of-phase, providing an under-damped response.

From the analogue systems described, the equation that governs the electrical and mechanical system is shown:

$$VI = \omega_{error}\, T_{damping} \tag{50}$$

The equation summarizes the previous discussion where voltage and current in the RLC circuit equates to the speed error variation, ω_{error}, and the torque component, $T_{damping}$, of the rotational motion system. Figure 35 shows the two waveforms that will be associated with the RLC circuit and their respective system responses.
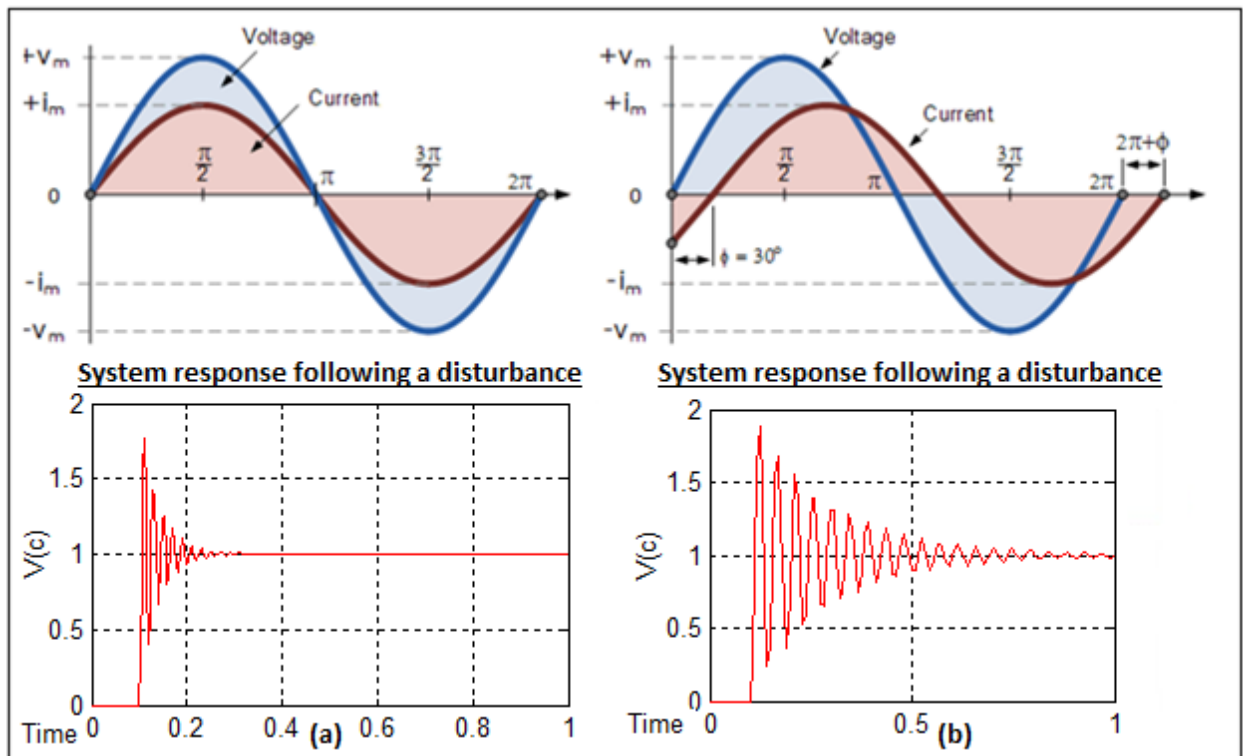
Figure 35: Waveforms for voltage and current being in and out-of-phase for a RLC circuit.

42

Figure 35-(a) shows what occurs when the voltage and current waveforms being perfectly in phase during a disturbance. The system damps the disturbance as quickly as possible to return to a steady state with minimal oscillations due to minimal energy interaction between the capacitor and inductor.

Figure 35-(b) shows what occurs when the voltage and current waveforms are slightly out-of-phase and the damped system response beneath. During a disturbance, there is energy transfer occurring between the capacitor and inductor for a longer duration. As a result, power is dissipated across the resistor resulting in the damped oscillations being more pronounced when compared to the ideal damped response resulting in the system taking a longer time to return to a steady state condition.

From Figure 35-(a), there is minimal energy interaction between the inductor and capacitor and the majority of the power is dissipated across the resistor. In this state, the system provides an ideal damped response, damping the power with minimal oscillations and returning the system to a steady state as quickly as possible.

The under-damped and ideal damping will transfer into a mechanical system as well. Figure 36 shows what occurs when the speed error variation and damping torque waveforms are in-phase versus a system with a where the damping torque is applied slightly out-of-phase with the speed variation.
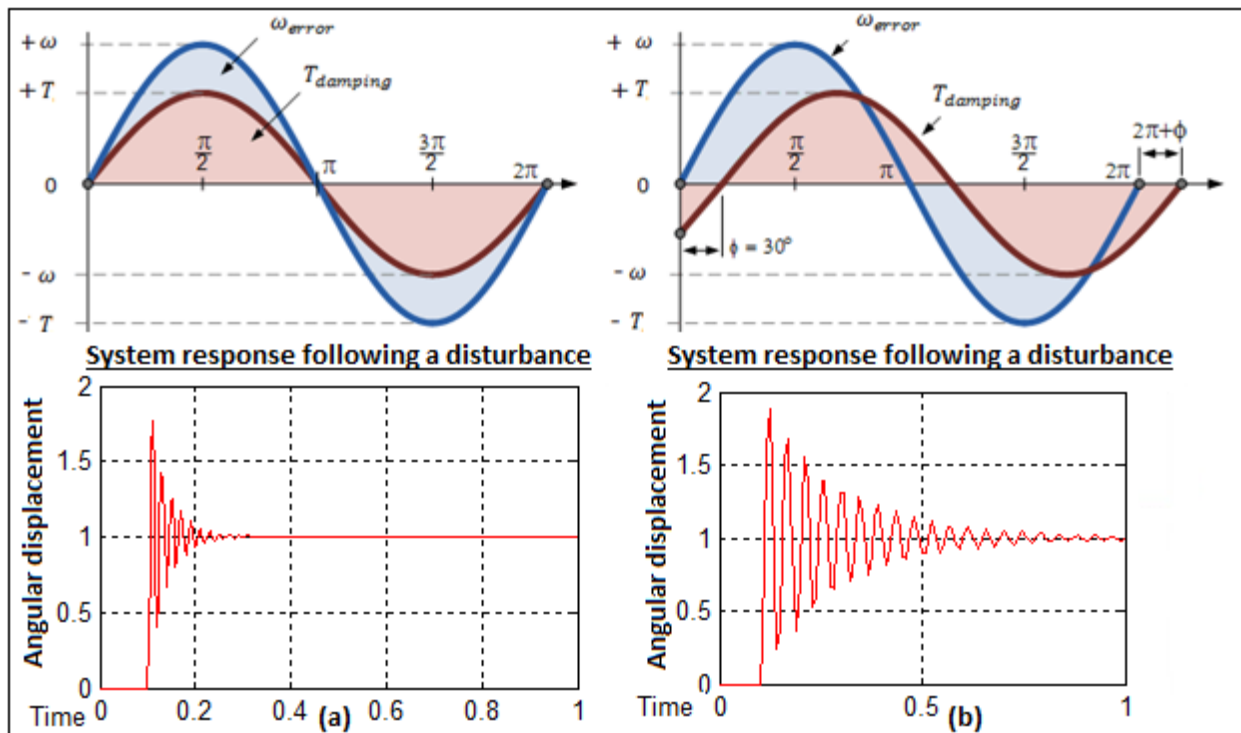
Figure 36: Damping Torque and speed variation waveforms showing in and out-of-phase for a mechanical system.

When observing at how a damping torque is supplied via a VSD in a mechanical system based on the RLC circuit approach, the motor damper windings will be briefly discussed.

During a steady state condition, the rotor speed is equal to the speed of rotation to the stator flux, the damper circuits of the motor do not cut the magnetic flux and therefore have zero current flow. However, during a transient condition, when a speed variation error occurs, the damper circuits have relative motion with respect to the generator magnetic flux. As a result of the rotor speed being different from the stator flux speed, flux cutting occurs, an emf is generated and current flows.

In Figure 36-(a), a torque is applied that is in-phase with the speed variation error waveform, this torque is referred to as the damping torque component or damping reference. The VSD generates this damping torque by acting as a current source by injecting current into the system that is in-phase with the speed variation component into the system, which results in minimal oscillations.

The amount of current injected is obtained from external measurements to determine the speed difference. The VSD then produces a torque component on the rotor which is in-phase with the speed difference. This injected current generates the damping torque. The VSD representation of a current source is the same as the current source analogue that was noted in Figure 34.

With the two waveforms being in-phase, the system is in a condition similar to that of the RLC circuit of Figure 35-(a), providing an ideal torque damping component resulting in minimal oscillations.

The majority of the damping power is dissipated across the resistance component of the system. In the mechanical system, the VSD acts as the damper, with the power being dissipated across the drives brake resistor.

The power is dissipated across the brake resistor to ensure an ideal damped response. This ensures that the system returns to a steady state condition from the transient condition with minimal oscillations.

In a generator system, the stiffness of the shaft is what causes the speed error between the generator and shaft, i.e. the oscillation disturbance. It should be noted that as the amplitude of the speed error varies, the amplitude of the damping torque will vary as well, such that the damping torque component provided by the VSD can be described as a modulating torque.

Figure 36-(b) shows what occurs if the damping torque waveform was supplied slightly out-of-phase with the speed variation waveform, the power would still be dissipated across the damper element. However, in this case, as a prolonged exponentially decaying oscillating waveform. This is as a result of some energy transfer occurring between the spring and mass mechanical components and taking longer to return to a steady state, in this case the VSD drive is supplying an under-damped, damping torque.

From the above discussion, an oscillating electrical LC and a mechanical spring circuit assuming zero resistance was described. Using first principles, an analysis was done on how the two systems analogues relate to one another. The discussion then moved onto how looking at these systems act realistically by adding a resistive component that dissipates energy and how both systems are affected.

The translation was then used to serve as a frame work to move onto a rotational motion system and how the electrical analogue system compares. Finally, it was noted from table 9.3.1, how the analogues for torque and speed for a rotational system of motion translates to that of voltage and current for an electrical system.

With the rotational motion system and electrical analogue circuit translation obtained, the methodology will be applied to a wind turbine generator system. A mechanical approximation of a wind turbine model will be formed based on the rotational motion system analogue with the VSD acting as the damper element. The methods described of how, following a disturbance, i.e. turbulent wind disturbance, damping is achieved via the VSD supplying a torque component with the speed variation error.

9.4   Mechanical analogues of directly connected generators

In using the mechanical approximation described in Figure 32 and applying a first approximation approach to a wind turbine model, the behavior of a synchronous machine can be considered analogous to a torsional spring [22]. Torque is proportional to the angle of the rotor and to that of the stator field. This angle is referred as the load or power angle. When compared to that of an induction generator, it can be thought of as a torsional damper where the torque is proportional to the difference in speed between the rotor and stator field (i.e. the slip speed) [22]. A mechanical approximation of a wind turbine model is described in Figure 37.
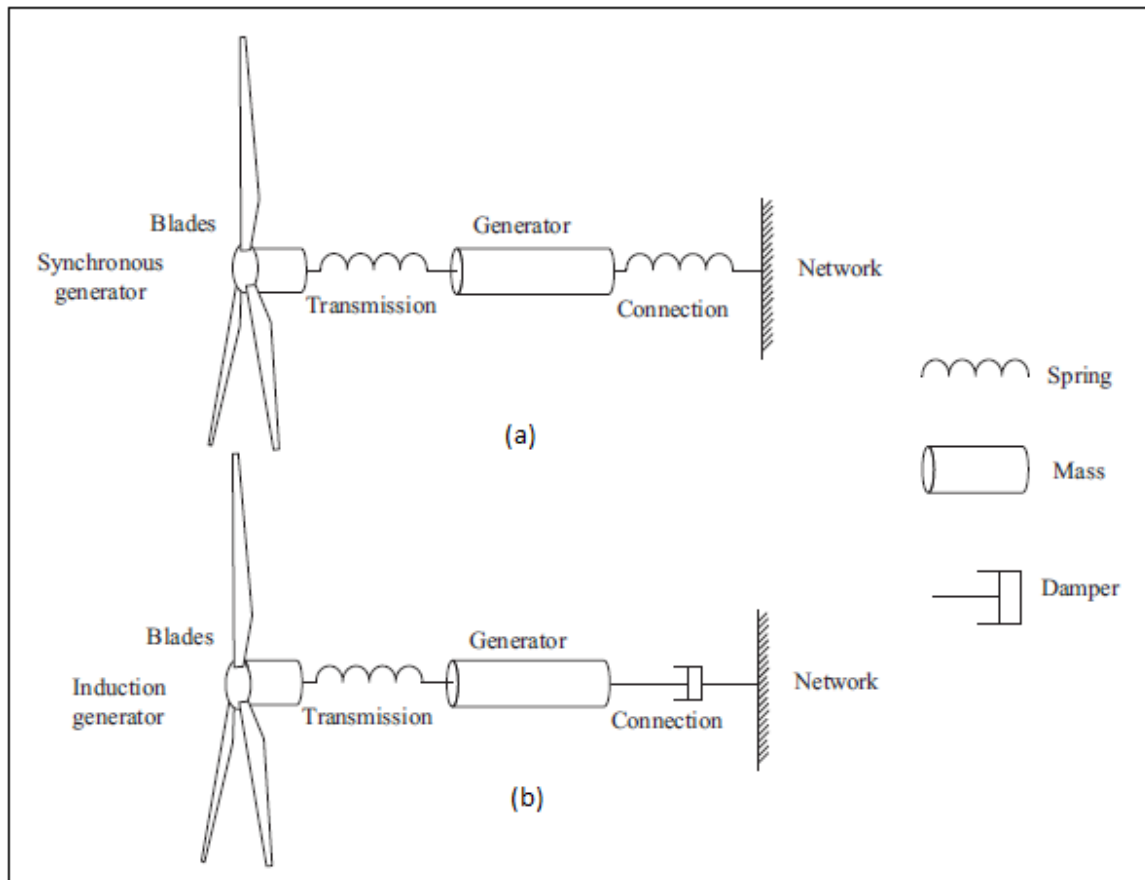
Figure 37: Mechanical analogue of synchronous and Induction generators [22].
Image used with publisher permission.

It can be seen from Figure 37-a, the synchronous generator, is excited by a cyclic torque from the wind turbine motor, there is no damping energy extracted from drive train to control torsional oscillations. As this system is a 2-spring, 2-mass system.

Examining Figure 37-b, the Induction generator, the connection of the generator to the network is represented with a torsional damper [22]. The cyclic torque of the wind turbine rotor will be at blade passing frequency and this often closely matches the natural frequency of oscillation of a synchronous generator connected to a network.

The generator of a variable speed wind turbine is not connected directly to the electrical network, but is instead de-coupled from the network. Based on the mechanical analogue, the torsional damper can be represented by an external resistor connected to the rotor circuit or a VSD. Varying the speed when using the external resistor involves a technique referred to as variable slip operation.

9.4.1 Variable slip operation

Variable slip operation is in-between that of fixed and variable speed operation. The variable slip generator is an induction generator with a variable resistor in series with the rotor circuit. This resistor is controlled by a high frequency semi-conductor switch [22]. Below rated torque or power, the external resistor is short-circuited and the generator acts as a conventional fixed speed induction machine.

Above rated torque, varying the resistance allows the generator torque to be controlled and the generator speed to increase [22]. In this configuration the system behaves similar to that of a variable speed system. A steady state equivalent circuit of variable slip induction generator with an external variable resistor is shown in Figure 38.
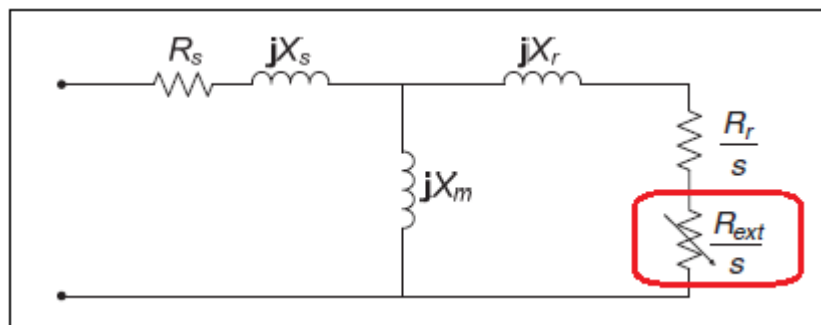
Figure 38: Variable slip induction generator equivalent circuit with an external variable resistor highlighted [22].
Image used with publisher permission.

When comparing the circuit to that of the RLC equivalent circuit, the external resistor is representative of the resistor in the circuit, the generator would be representative of the inductor, while the capacitor is equivalent to that of the transmission component. The components are matched to the damper, mass and spring respectively, as described in Figure 37-b. Varying the value of the external resistor, would vary the current (i.e. torque, in the mechanical equivalent) in the system.

The external resistor configuration has the advantage of controlling the torque in the drive train and smoothing out aerodynamic torque variations above rated power at a cheaper rate than a variable speed system, but it is not a true solution.

The main disadvantage of the external resistor system is that is does not allow the control of power factor [22].

By utilizing an external resistor connected to the rotor circuit, the entire power circuit is mounted on the shaft (including the external resistor and power electronics). Mounting the external resistor in such a configuration, allows any extra heat generated by the resistor to be dissipated.

9.4.2 Variable speed operation

By using frequency conversion between the generator and the network, it is possible to de-couple the rotational speed of the generator and turbine from the network frequency [22]. This allows the rotor speed to vary in order to maximize energy capture. The generator air-gap torque can be accurately controlled while reducing mechanical loading [22].

By using a wound rotor induction machine and replacing the external resistors in the rotor circuit with a frequency converter (i.e. the frequency converter now acts as the damping component in the mechanical analogue) it would be possible to vary the speed of an induction generator. This is referred as a Double Fed Induction Generator (DFIG). With a frequency converter now between the generator and network, the equivalent circuit now changes that shown in Figure 39.
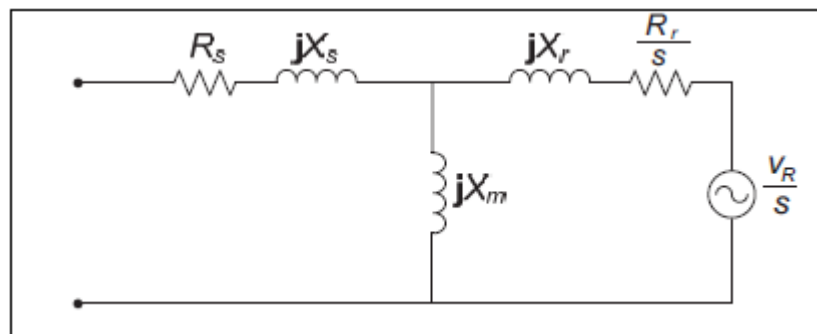
Figure 39: Steady state equivalent circuit of the DFIG [23].
Image used with publisher permission.

A development of the variable slip system is to replace the variable external resistor with that of back-to-back frequency converters [23]. These converters apply a variable voltage (by injecting current) at the rotor slip frequency and so allow operation above and below the synchronous speed of the stator field. The synchronous speed of the stator field is determined by the network frequency and the number of poles in the stator winding.

It can be seen from Figure 39, that the external variable resistor has been replaced with a voltage source. This applies a voltage to the slip rings of the wound rotor at slip frequency. The equivalent circuit has the rotor circuit referred to that of the stator such that the injected rotor voltage is divided by slip.

With rated applied torque, the speed may be adjusted by varying the injected voltage into the rotor circuit [23]. When mechanical oscillations occur, the converter applies a corrective signal by varying the torque such that the torque oscillations are counter-acted.

The use of a frequency converter when de-coupling the generator from the network in place of the external resistor has the following advantages:

- Below rated wind speed, the rotor torque can be varied to maintain peak aerodynamic efficiency;
- In the event the turbine blades approach a speed that they aren't designed to handle, the rotor is able to act as a flywheel to prevent torque fluctuations from entering the drivetrain;
- The VSD is able to precisely control the air-gap torque. This allows gearbox torque variations to be kept at a minimum. This allows the VSD to provide a damping torque to eliminate oscillations;
- Reactive and active power can be controlled, such that a specific power factor can be maintained. An example of this would be using the wind turbine as a reactive source to compensate for poor power factors of other consumers on the network, and;
- A variable speed controlled wind turbine can give a higher quality of power due to the smoother output power they develop.

With larger turbines, variations in aerodynamic torque at the blade passing frequency can be significant. This is due to the size of the rotor compared to the lateral and vertical scales of turbulence. The turbine control system can be tuned to allow the aerodynamic power variations to be absorbed as small changes in rotor speed, i.e. as variations in kinetic energy [22].

Two methods are employed to achieve variable speed operation, broad and narrow range variable speed operation. In broad range, the generator stator is connected to the network via two fully rated frequency converters. In narrow range, variable speed is achieved using a DFIG, both the generator and stator are connected to the network [22]. The stator is connected directly and the rotor is connected via slip rings and smaller frequency converters. In both methods, the control system measures the generator rotational speed and applies the torque required to keep the aerodynamic rotor at an optimal speed at wide range of wind speeds.

An example of the narrow range configuration using frequency converters is shown in Figure 40.
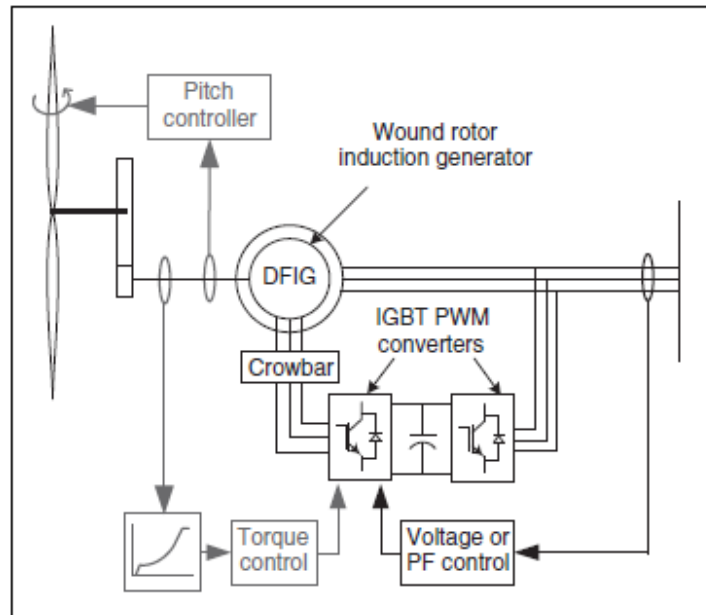
Figure 40: Narrow range operation using a DFIG [22].
Image used with publisher permission.

In the above configuration, the controllable rotor resistance is replaced with back-to-back converters used to connect the rotor to the network [22]. This gives the variable speed operation to be done over a specific speed range depending on the direction of the power flow in the rotor circuit. This configuration prevents energy to be dissipated in an external rotor resistance. Control of the generator speed and power factor is done by the rotor side converter, while the network side converter maintains the DC link voltage. With broad range operation, all the power from the generator in rectified to DC in the arrangement shown on Figure 41.
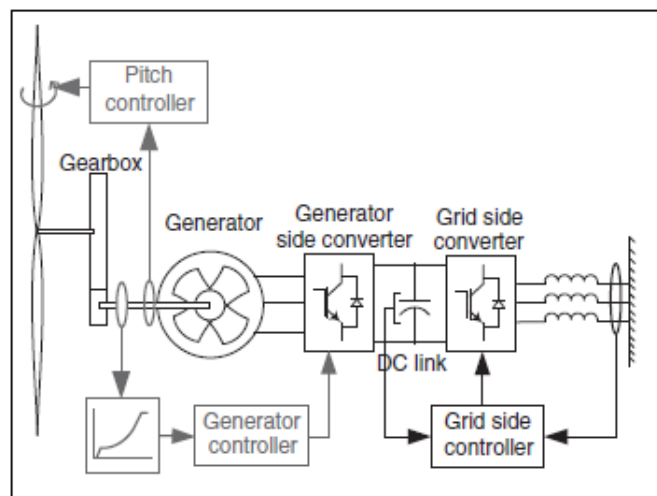
Figure 41: Broad range operation using full power control [22].
Image used with publisher permission.

With broad range operation, control of the generator torque is done via the generator side converter. The grid side converter maintains the DC link voltage. An additional function of the network side converter can be used to control the network voltage or reactive power flow into the network [22].

9.5   Wind Turbine torsional damping via a Variable Speed Drive.

A major cause of breakdowns in wind turbine generators are damages in the drive train which is highly stressed by oscillations due to fast changes in wind speeds. These oscillating wind speeds especially affect the gearbox and bearings of wind power plants. The VSD controls the generator to prevent any unwanted torque components from entering the gear box. To minimize the drivetrain wear and tear, the focus of unwanted torque is based on removing the torque components near the natural frequency of the drivetrain by introducing a compensating torque in the generators electromechanical torque [24].

The torque difference between the aerodynamic torque on the turbine rotor and the generator torque acts on the gearbox resulting in mechanical stresses. Compensating torque of the generator can cancel out these harmful torque components from the torque difference, such that mechanical stresses reduce while increasing gearbox lifespan [24]. The generator-side power converter controls generator currents in such a way that provides variable speed wind turbine operation while reducing mechanical stress on the drivetrain. The principle of the proposed mechanical stress reduction strategy is illustrated in Figure 42.
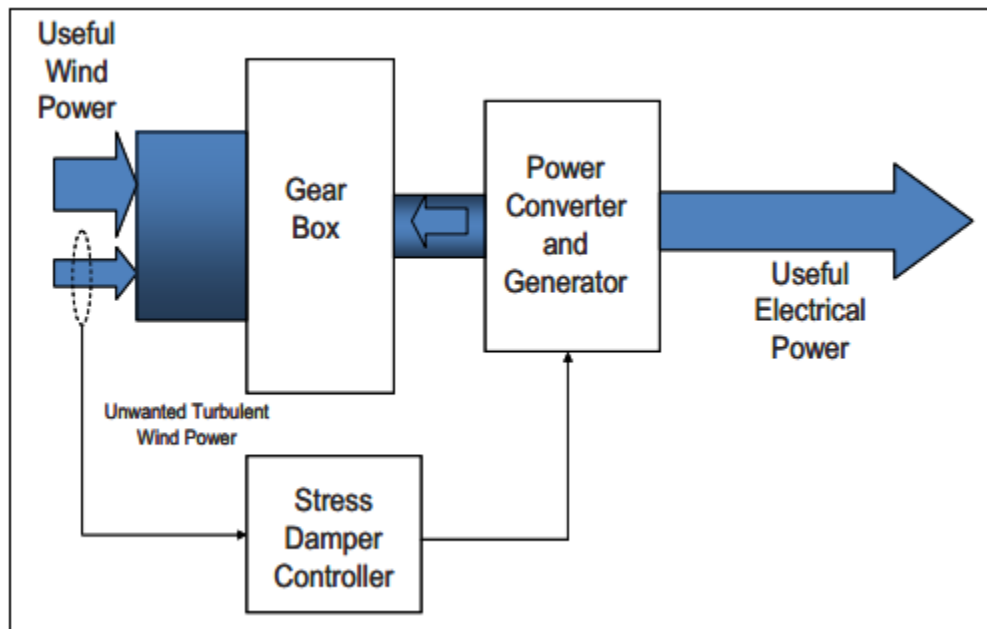
Figure 42: Energy flow diagram showing gearbox stress reduction [24].
Image used with publisher permission, Copyright © 2011, IEEE.

51

A drivetrain on a wind turbine generator normally consists of a large rotor inertia and a smaller high speed shaft inertia which is separated by a torsional spring which is representative of the twisting of shafts and couplings [25]. In a fixed speed turbine, the induction generator slip curve shown in Figure 43, acts like a damper, with torque increasing with speed.
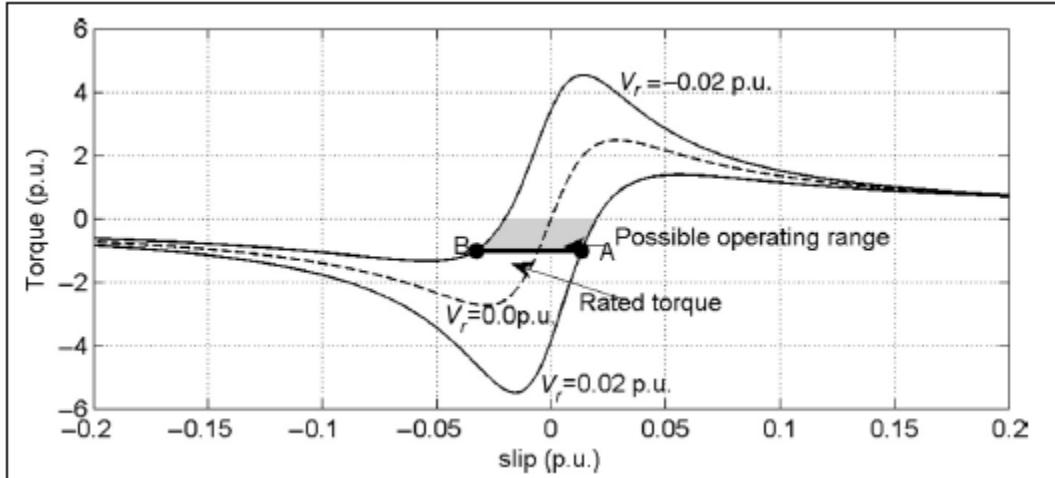
Figure 43: Torque slip curve of an induction generator [25].
Image used with publisher permission.

In a variable speed turbine operating at constant generator torque however, there is little damping, since the torque no longer varies with generator speed [25]. There is a small amount of structural damping in shafts and couplings, and some damping from the gearbox, but these effects contribute typically only a small fraction of 1% of critical damping. The very low damping can lead to large torque oscillations at the gearbox [25].

It is possible to provide further damping mechanically, for example by means of appropriately designed rubber mounts or couplings. It is difficult to provide enough damping and with additional damping elements this involves higher costs.

A solution is the use of a VSD to modify generator torque control to provide damping. Instead of demanding a constant generator torque above rated torque, a small torque ripple at the drive train frequency is added onto the basic torque reference such that the torque controller calculates a small corrective signal. The phase is adjusted to counteract the effect of the resonance and effectively increase the damping [25].

A simulation was done on a variable speed turbine with turbulence added. A before and after damping via a corrective signal is shown in Figure 44.
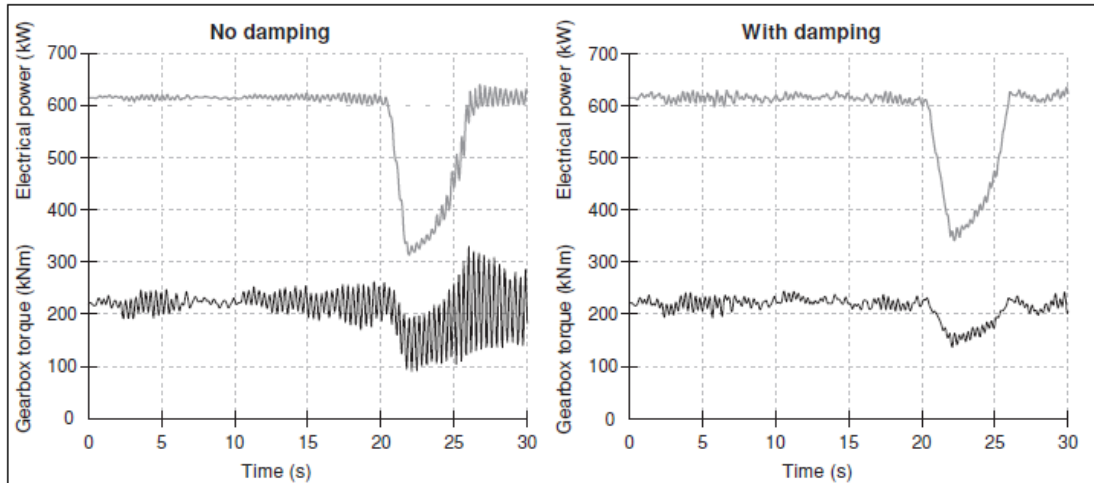
Figure 44: Effect of damping on a drivetrain [25].
Image used with publisher permission.

From the above figure, a large drive train resonance can be seen to be building up. Although the power and generator torque is smooth, the gearbox would be affected. The disturbance is almost completely damped without increasing the electrical power variations. This is because the torque ripple needed to damp the resonance is actually normally small, as the level of excitation is small as well [25].

The drive train damping can be improved by using an input signal representative of the "twisting speed" rather than just the generator speed. The twisting speed is the difference between the generator speed and the rotor speed (scaled by a gearbox ratio). This requires two speed measurements. With the twisting speed reference, the VSD essentially supplies a modulating torque. An example of average twisting speed across the shaft is demonstrated in Figure 45. The figure's representation of the twisting speed is exaggerated for the purposes of explanation.
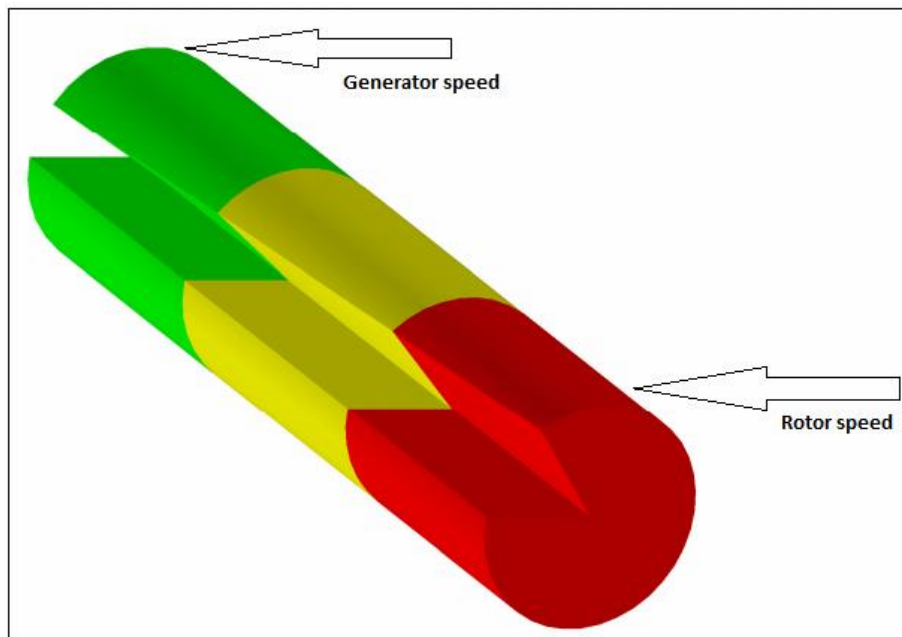
Figure 45: Generator speed vs. Rotor speed.

The speed difference between the rotor and the generator will be used to apply the corrective signal to the VSD. As power is a function of torque and speed, the small speed difference is what would cause unwanted vibration on the drivetrain which will be damped via the VSD. From this, a block diagram can be used to describe how the VSD integrates with a typical wind turbine model. The block diagram is shown in Figure 46.
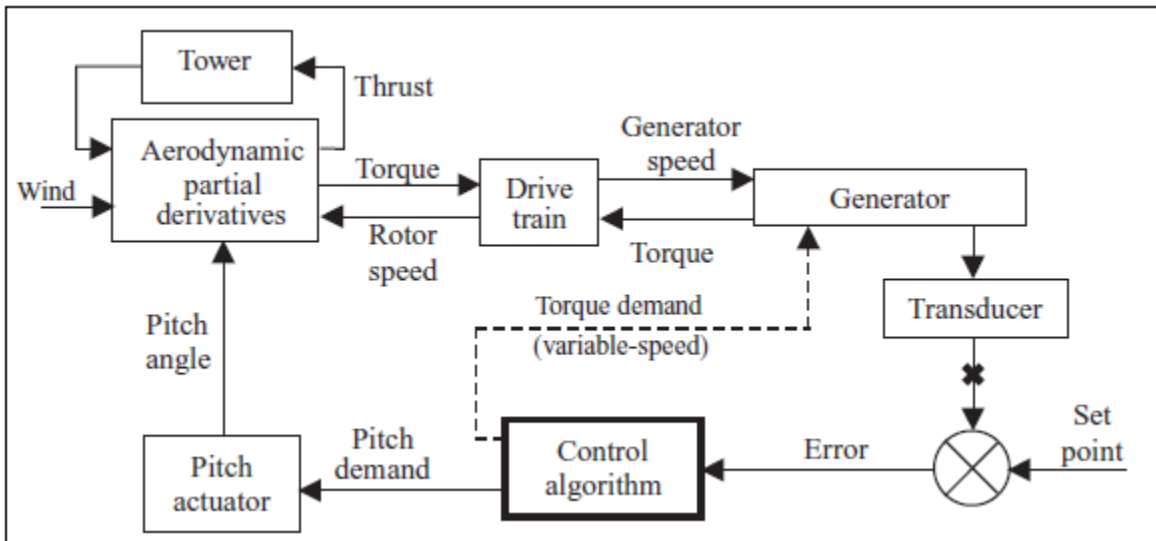
Figure 46: Typical Wind turbine model with a VSD configuration [25].
Image used with publisher permission.

10   Simulation

The simulation will utilize a corrective signal feedback approach described to provide a damping torque. The VSD will be connected to a motor. The motor and load shafts are assumed to be connected via rigid coupling. The motor and load shafts are also assumed to be solid. The assumptions for the mechanical parameters for the shafts and coupling are made to avoid torque transmission loss between motor and load during simulation. A damping torque is provided in response to shaft oscillations that occur from a torque pulse disturbance applied to the load section. To counter the shaft oscillation, the VSD supplies a damping torque based feedback from the speed variation as a result of the disturbance. The VSD provides a damping torque component to match the speed variation and damp the oscillations. The motor in the simulation has the following parameters:

- Power: 150 kW;
- Voltage: 460 V (Vrms);
- Nominal speed, N_m : 1800 rpm;
- Frequency: 60 Hz;
- Number of poles: 4;
- Rs = 14.85 mΩ;
- Rr = 9.295 mΩ;
- X_{ls} = 113.85 mΩ;
- X_{lr} = 113.85 mΩ;
- X_m = 3.943 Ω, and;
- Rotor inertia: 3.1 kg-m^2

10.1   The Simulink model

For the simulation, three scenarios will be investigated. The first will be the transmitted torque with an oscillating disturbance resulting from a torque pulse with no correction to serve as a base. A single 200 Nm torque pulse of one second duration is injected into the load inertia to establish a shaft oscillation. The pulse is introduced into the system after two seconds once the motor has reached 1800 rpm. The second scenario will be the transmitted torque with a corrective signal being applied with a small amount of torque being provided by the VSD based on the speed variation to demonstrate a degree of damping.

The third will be with the same corrective signal with the VSD supplying an increased torque component applied with the speed variation. This is to demonstrate how the damping increases by increasing the torque in the corrective signal. The Simulink model together with a simple load and mechanical shaft is shown in Figure 47. The first set of results will be bases on a 7 Hz disturbance. Two follow up results will demonstrate damping with a 3 and 20 Hz oscillation disturbance and the performance of these scenarios will be compared with each other.
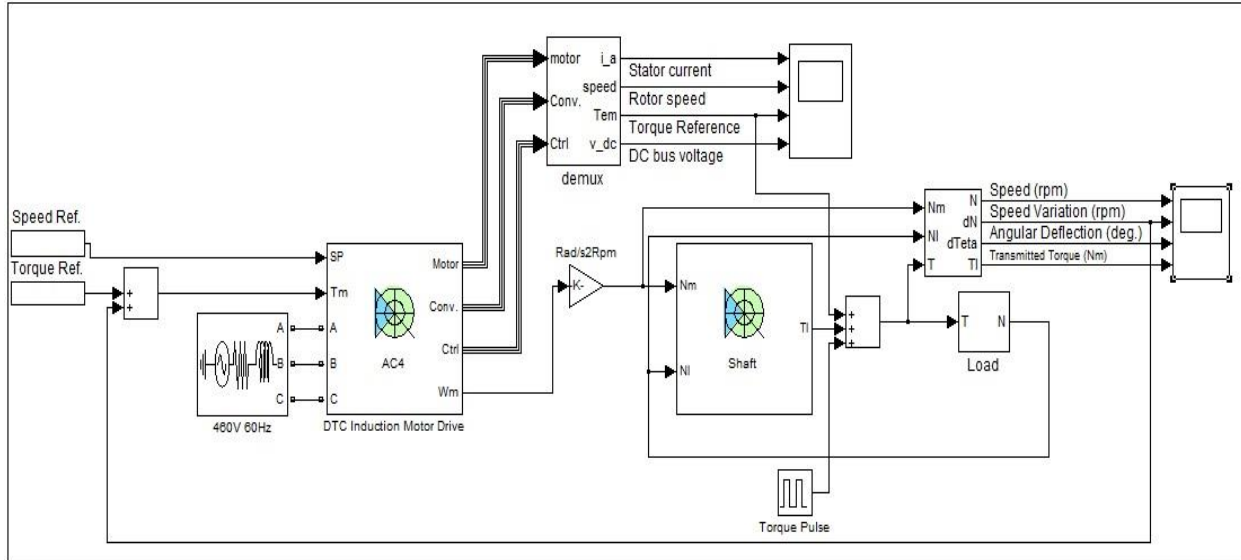
Figure 47: Simulink Model.

10.2 Simulation pre-calculation

Prior to the simulation, the model and its parameters will be analyzed based on the theory discussed so far. Theoretical calculations will be done to observe how the shaft and load parameters react to a 200 Nm torque pulse being applied to the load. When the system response with no correction via Simulink is completed, the response will be compared to the theoretical component to ensure that the result when applying a disturbance is as expected. The shaft and load from the Simulink model have the following parameters.

- The load has a Moment of Inertia, J, of 1 kg-m^2 with a viscous damping, D, parameter of 1 N-m-s/rad, and;
- The spring stiffness, K, of the motor and load shaft, has a parameter of 1719 N-m/rad.

As the oscillation will be dependent on the Moment of Inertia, it was chosen to be a low value in order to provide an observable oscillation in the response. With the shaft and load parameters on hand, the rate of oscillation for a rotational system can be calculated by utilizing equation 49.

$$\omega = \sqrt{\frac{K}{J} - \left[\frac{D}{2J}\right]^2} \tag{49}$$

$$\omega = \sqrt{\frac{1719}{1} - \left[\frac{1}{2(1)}\right]^2}$$

$$\omega = 41.45 \; rad/s$$

From the result of equation 49, applying a disturbance will result in an expected oscillation frequency of approximately 7 Hz.

56

Utilizing the angular speed calculation above, the transient solution for a rotational system, with no driving torque, can be translated from equation 40.

$$\theta = A e^{\frac{-Dt}{2J}} \cos(\omega t) \qquad (51)$$

The system response with no correction is expected to have a slight decaying oscillating response. This is as a result from the system having a small component of damping from the viscous damping component. If no damping component was present, the system would oscillate indefinitely from the applied disturbance showing no decay.

A single torque pulse is applied to the system. The torque pulse with the one second duration is shown in Figure 48.
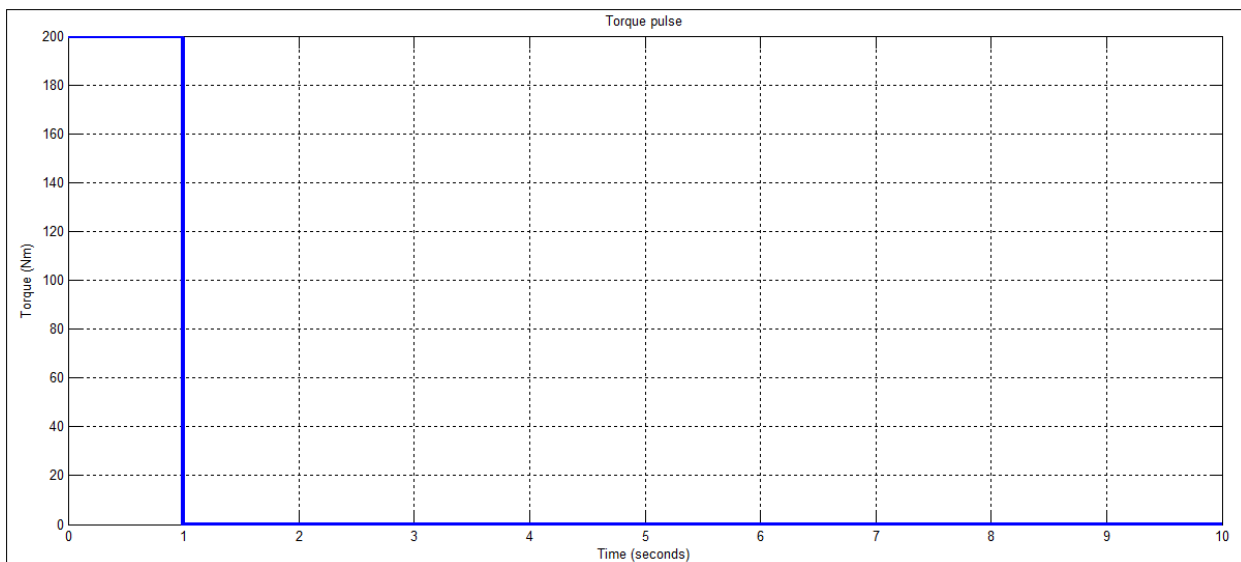
Figure 48: Pre-calculation Torque pulse.

The torque pulse is applied to the load from an external disturbance. This can be in the form of the shaft being clamped for a second and released. For the theoretical calculation, the disturbance is applied and the system response is observed. The predicted response with no correction is shown in Figure 49.
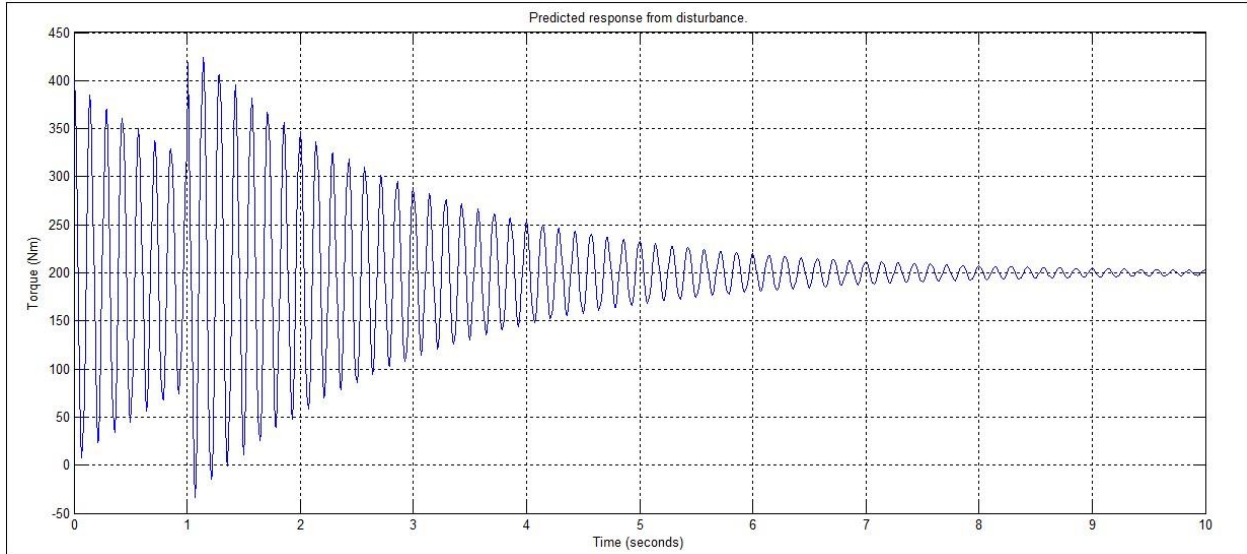
Figure 49: Pre-calculated system response from disturbance.

From the above figure it can be noted that the frequency of oscillation corresponds with what has been calculated as a result of a low Moment of Inertia. The waveform is oscillating at the calculated rate of 7 Hz while undergoing a slightly damped decaying response, this also corresponds with the theory discussed as the load and shaft parameters have a low viscous damping and spring coefficients. The response shown in Figure 49 is the predicted response on what should occur for the Simulink model for the first scenario when a torque pulse is injected into the load, inducing an oscillation with no corrective feedback. With the predicted oscillation calculated, the Simulink model will now be analyzed.

10.3 Simulation via Simulink

The system response on the Simulink model will be analyzed based on a single torque pulse being injected into the load from an external source. The motor reaches its rated speed after two seconds. The torque pulse is applied at this time. The torque pulse is shown in Figure 50.
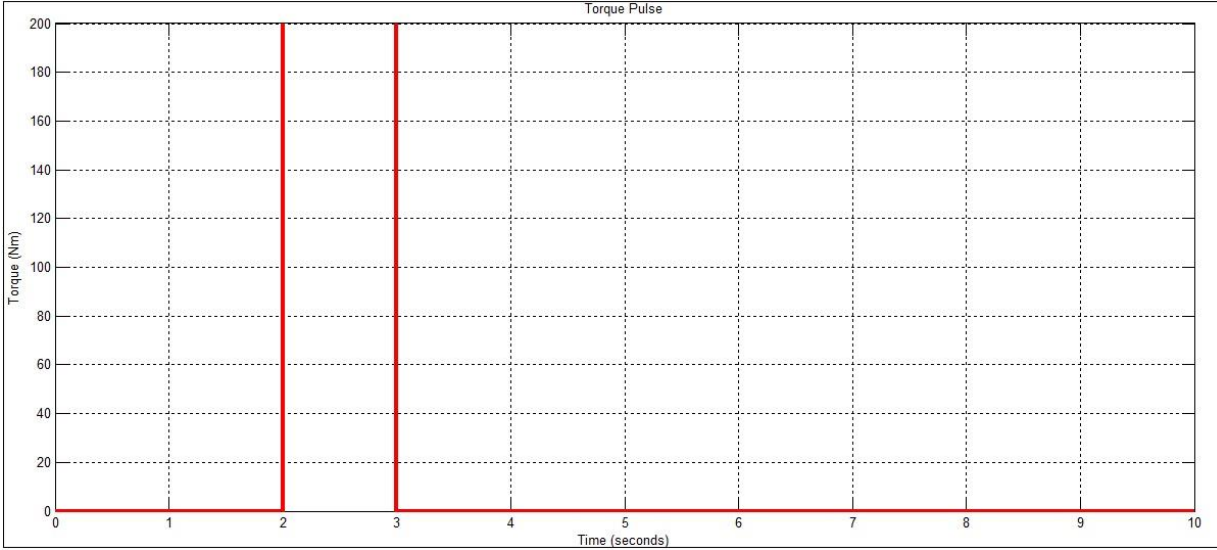
Figure 50: Torque pulse with one second duration.

The configuration of the DTC induction motor drive is made up of several components. These components include the variable speed drive with the DTC component and the motor itself. The configuration of the direct torque controlled motor drive is shown in Figure 51 with the inverter in blue and the DTC subsystem shown in green.
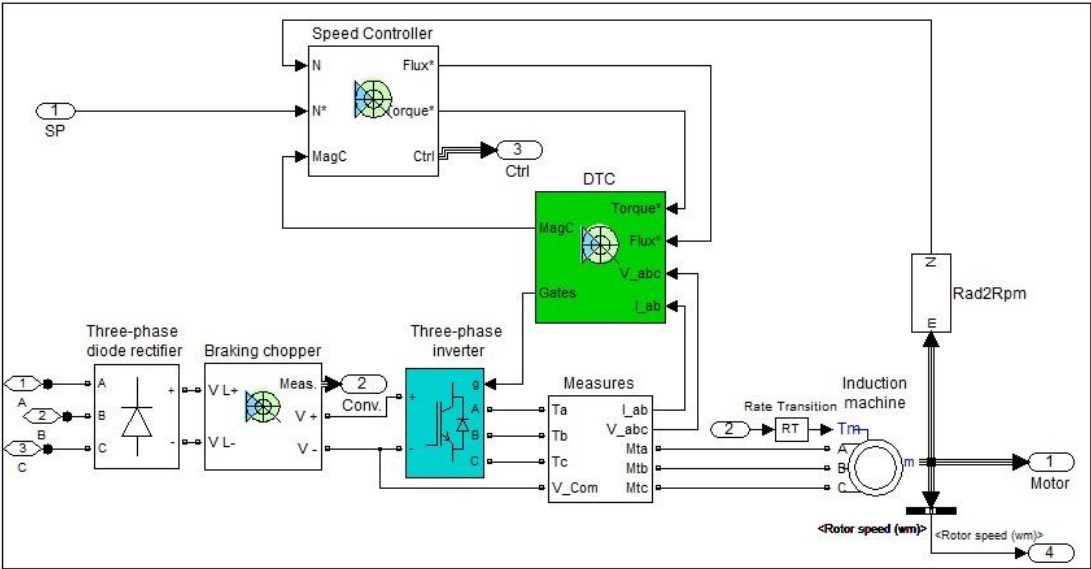
Figure 51: Components of the DTC system.

59

10.4 System response from a disturbance with no torque correction

The simulation is run over 10 seconds. The torque pulse is then introduced into the load after two seconds into the simulation. The torque pulse induces a speed oscillation on the shaft. The oscillations in the shaft and transmitted torque are shown in Figures 52 and 53 respectively.
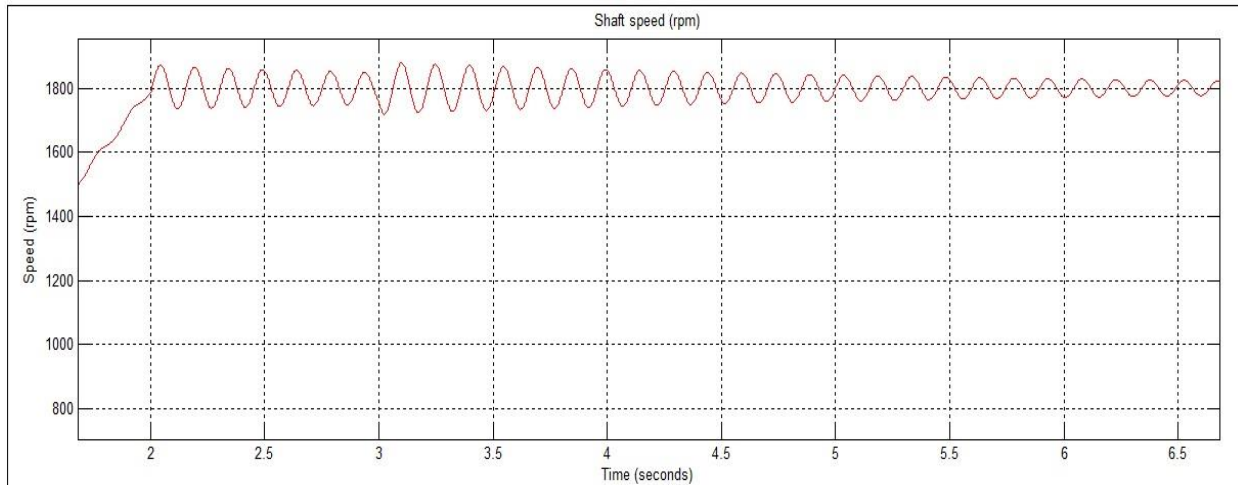
Figure 52: Shaft oscillation from torque pulse.
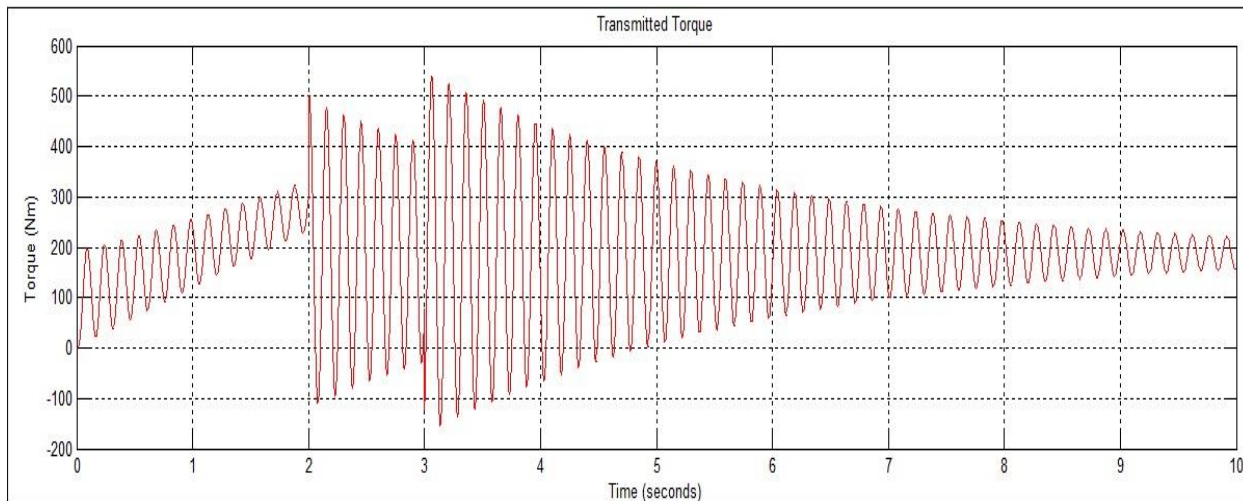
Figure 53: Transmitted torque with no correction.

From the above figures, it can be noted what effect a torque pulse can have on the motor shaft. An oscillation is introduced which affects the transmitted torque. The next step is to apply a corrective torque based on the speed variation.

10.5 System response from a disturbance with torque correction

For the second scenario, the same simulation is run with the same torque pulse being applied. However, in this case, a small torque value is applied based on the speed variation feedback. The results of the shaft speed and transmitted torque are shown Figures 54 and 55 respectively.
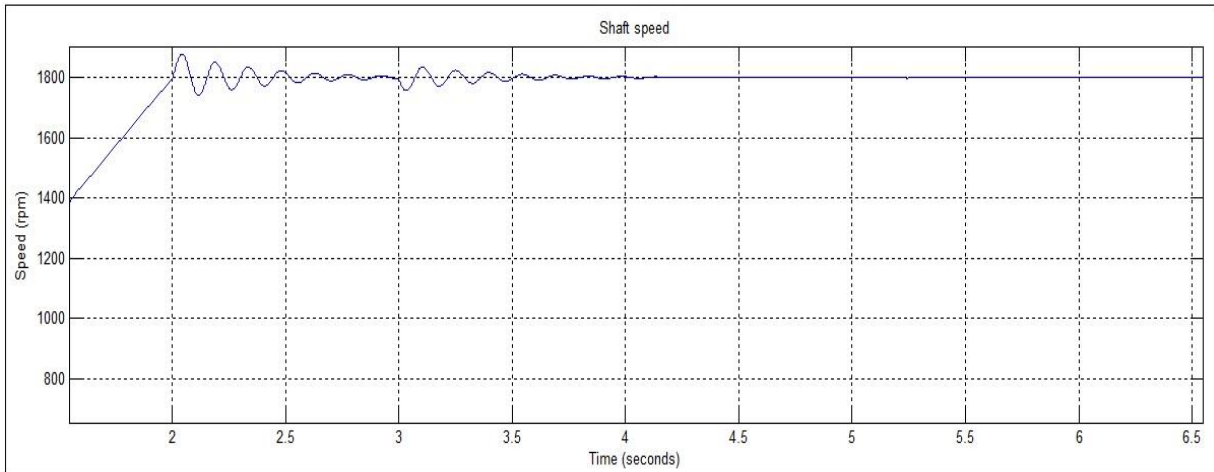
Figure 54: Shaft oscillations with torque corrective signal applied.
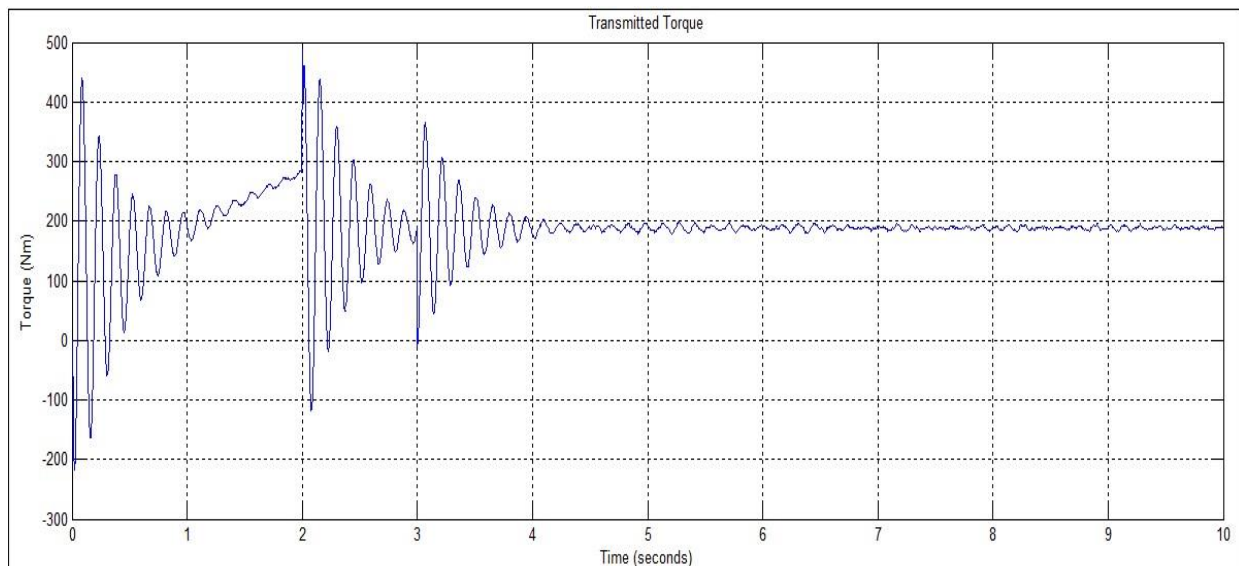
Figure 55: Transmitted torque with torque correction.

It can be noted that there is an improvement in the transmitted torque with the corrective torque applied with the speed variation. This however, is not ideal. To damp the disturbance further, the third scenario supplies an increased torque being applied with the speed variation.

10.6 System response from a disturbance with increased torque correction

The third scenario involves the torque corrective signal being applied with the speed variation, while in this case, with a larger torque being supplied. The results of the shaft speed and transmitted torque are shown in Figures 56 and 57 respectively.
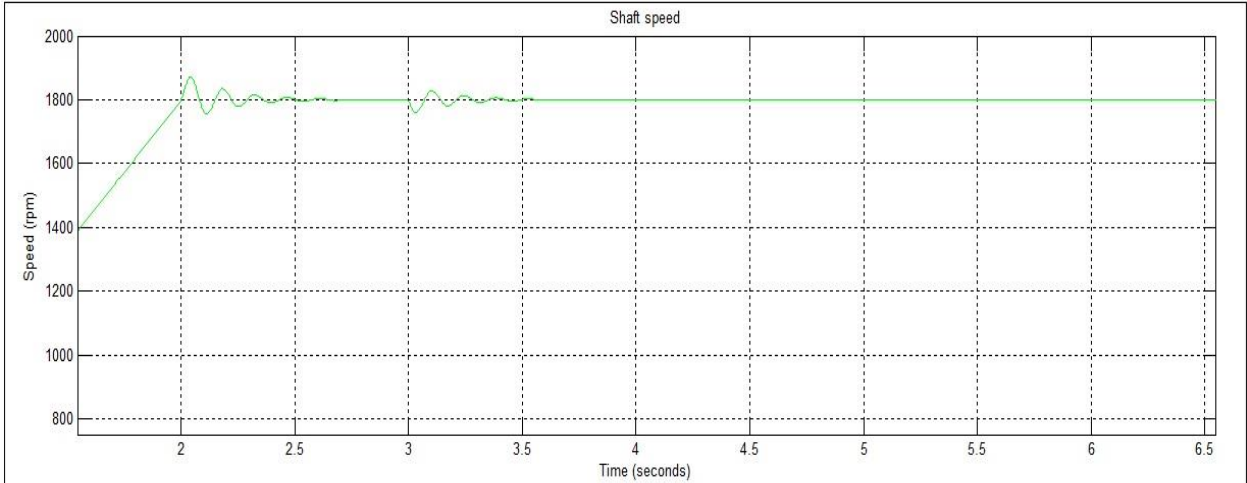
Figure 56: Shaft oscillations with larger torque corrective signal applied.
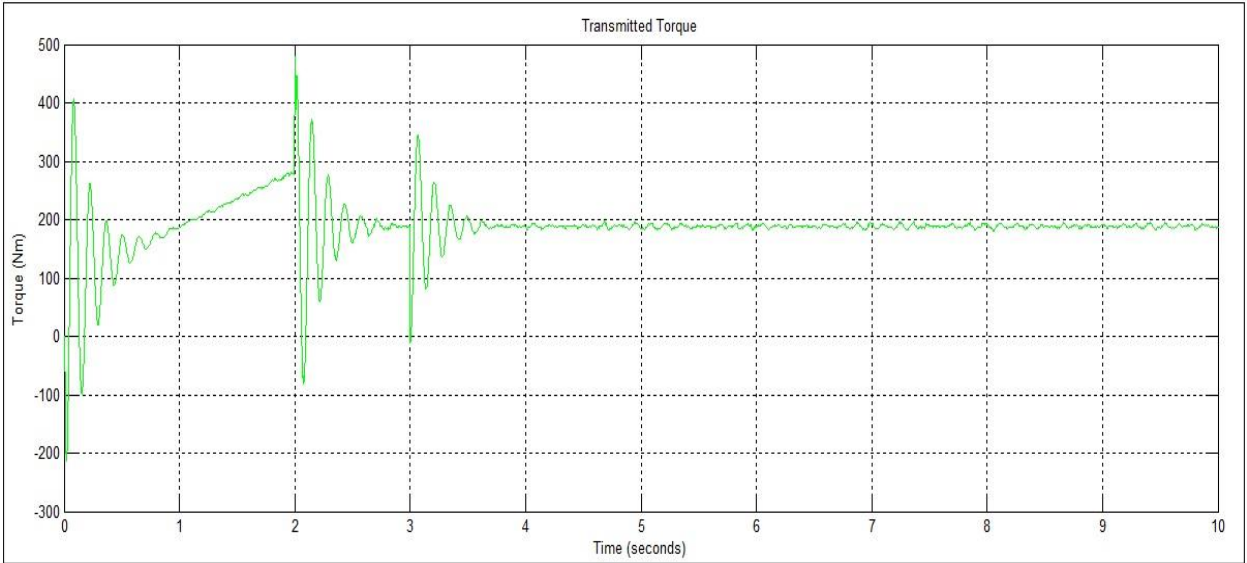
Figure 57: Transmitted torque with larger torque correction.

From this result is can be seen that the disturbance has been damped when compared to the original and previously damped disturbance. This demonstrates that applying a larger torque value with the speed variation results in increased damping.

10.7 System response with varying frequency oscillation

Two additional scenarios will be investigated and the damping performance will be compared to the previous result where a 7 Hz oscillation was used. The first case is observing the system performance with a 3 Hz frequency oscillation. With the system in the second case having a 20 Hz frequency oscillation.

10.7.1 Transmitted torque with 3 Hz frequency oscillation

In order to change the oscillation frequency, the Moment if Inertia is required to be adjusted. In this scenario the Moment of Inertia will be set to 4.8 kg-m^2. Using equation 49, the following result is obtained.

$$\omega = \sqrt{\frac{K}{J} - \left[\frac{D}{2J}\right]^2} \tag{49}$$

$$\omega = \sqrt{\frac{1719}{4.8} - \left[\frac{1}{2(1)}\right]^2}$$

$$\omega = 18.90 \, rad/s$$

Applying a disturbance with the above result to the simulation will provide an oscillation frequency of approximately 3 Hz. As with the previous simulation, where a 7 Hz oscillation was used, the same torque correction values are utilized and a summary of the transmitted torques is shown in Figure 58.
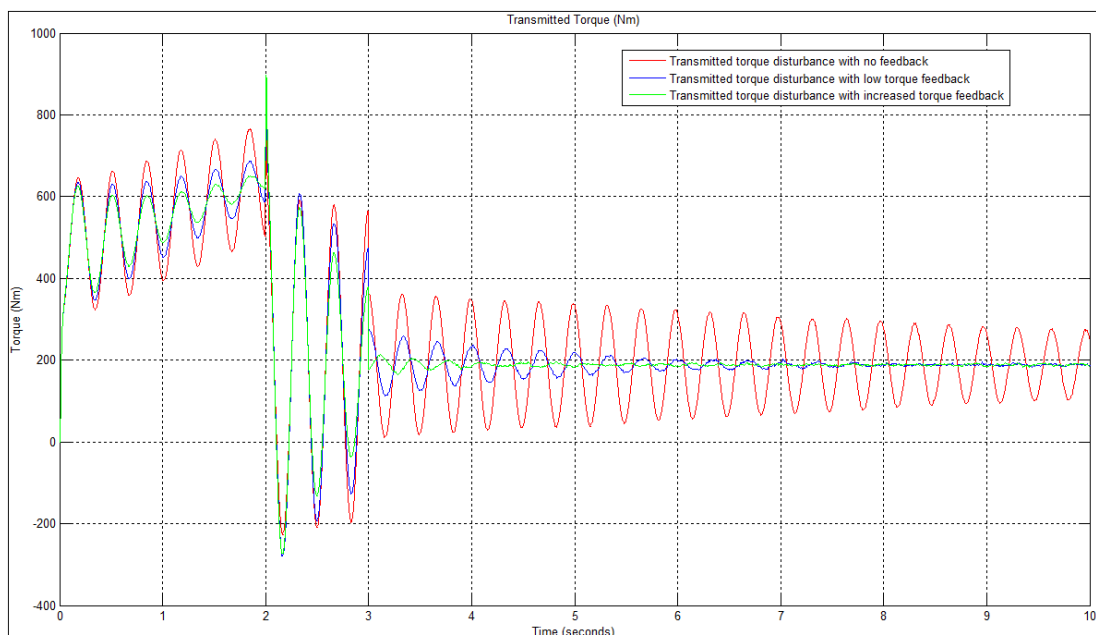
Figure 58: Summary of transmitted torques with varying damping states at 3 Hz.

63

10.7.2   Transmitted torque with 20 Hz frequency oscillation

For the second case of varying frequency, a higher oscillation frequency is chosen. The Moment of Inertia in this scenario is set to 0.1 kg-m². Using equation 49, the following result is obtained.

$$\omega = \sqrt{\frac{K}{J} - \left[\frac{D}{2J}\right]^2} \qquad (49)$$

$$\omega = \sqrt{\frac{1719}{0.1} - \left[\frac{1}{2(1)}\right]^2}$$

$$\omega = 131.10 \; rad/s$$

This parameter will result in a 20 Hz oscillation frequency. As with the 3 and 7 Hz scenarios, the same torque value correction parameters during the simulation are used. A summary of the transmitted torques is shown in Figure 59.
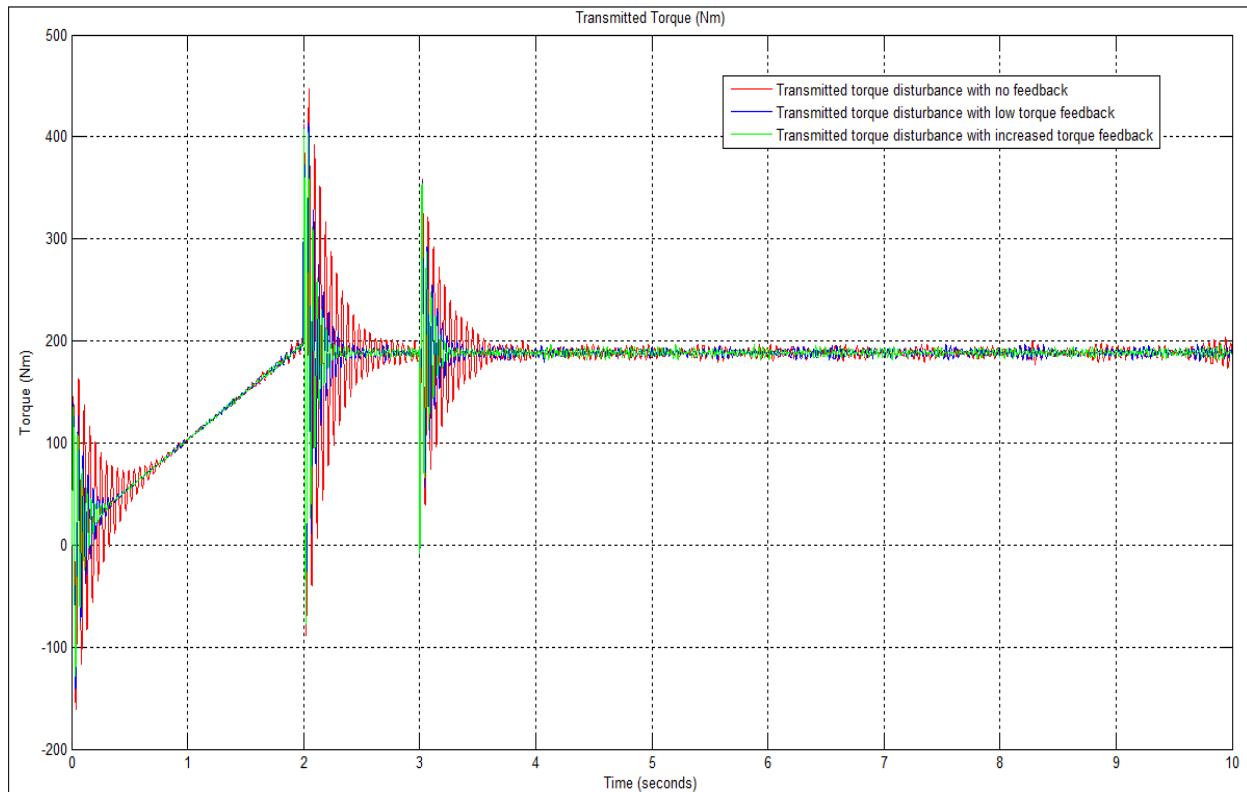
Figure 59: Summary of transmitted torques with varying damping states at 20 Hz.

11 Discussion of results

With the simulations on the various damping and frequency scenarios achieved, a summary of the torques from Figures 53, 55 and 57 utilizing the 7 Hz disturbance with their respective corrective signals and how damping is applied in each case is shown in Figure 60.
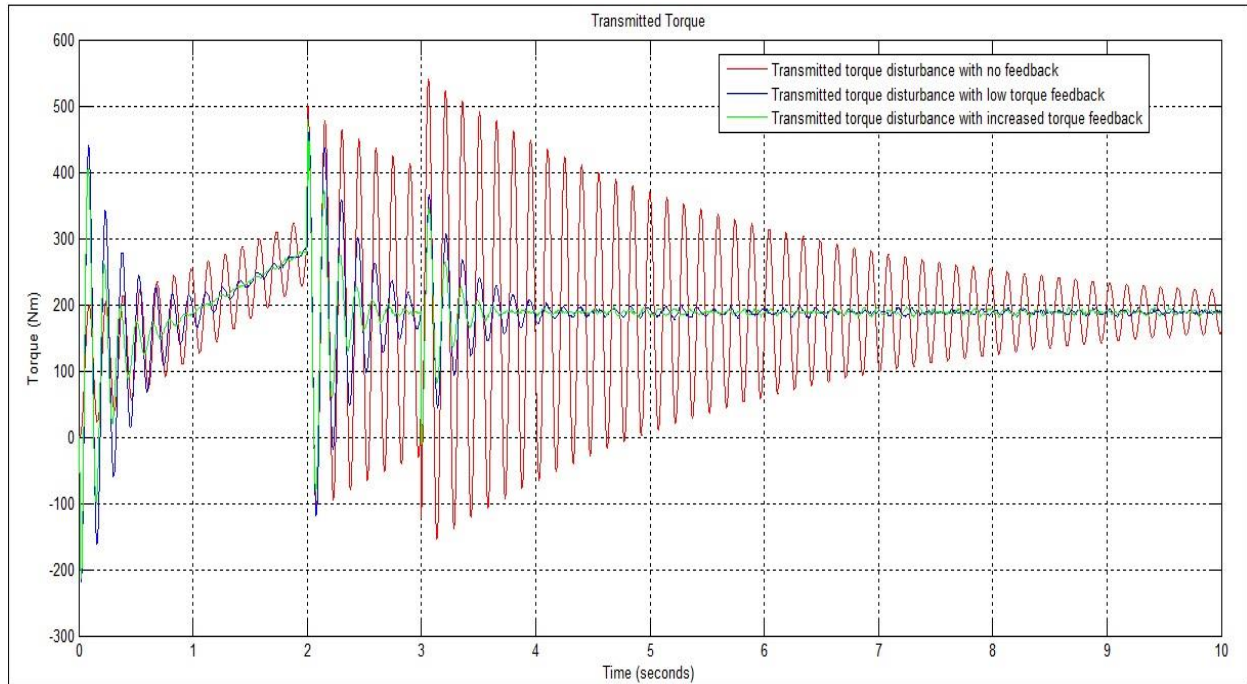
Figure 60: Summary of transmitted torques with varying damping states at 7 Hz.

With the simulation completed, it was shown that greater damping is achieved by applying a larger torque corrective signal with the speed variation. The speed variation was the result of a disturbance from an oscillating shaft which was caused by torque pulse being introduced to the system. With no corrective feedback, the disturbance passed through the system resulting in severe torque and shaft oscillations. When applying a small amount of torque with the speed variation, the torque oscillations were damped by approximately 60% after the initial disturbance. It can be observed from all three frequency oscillation scenarios, the damping performance remained consistent in each case.

With a larger torque applied, the torque disturbance was damped by further, by approximately 80% after the initial disturbance when compared to the torque disturbance case with no feedback. When the torque pulse ends, the system returns to a stable state within half a second, compared to over a second with second scenario. It can be noted from the torque response from the second and third scenario, there is still a disturbance in the transmitted torque. However the toque disturbance can be regarded as negligible when compared to the torque response with no feedback.

When observing the superimposed waveforms in Figure 60, three observations can be made. The first observation is that only the torque component as a result of the speed variation is affected. The overall torque from the torque reference of 200 Nm to the system is mostly unaffected. The second observation is that as the corrective torque is being applied to the speed variation, it results in an exponentially decaying sinusoidal waveform of the transmitted torque based on the disturbance. It can be noted that the pre-calculation waveform, Figure 49, with no disturbance feedback matches closely the disturbance waveform from the Simulink response shown in Figure 53. This is an indication that the system is behaving as it should when compare to the theoretical component.

The third observation is that the greater amount of torque being applied to the torque reference based on the speed variation results in increased damping and a faster settling time.

This increase in damping is due to when supplying an ever increasing torque to the speed variation, a greater amount of energy is being dissipated resulting in greater damping. The VSD will incur increased switching losses as a result of the VSD supplying increased current for the torque control component. When observing the energy flow, the drive is taking feedback based on the speed variation which in turn supplies a torque component. A smaller amount of damping power is supplied as the oscillations get smaller with each cycle. With the tolerance levels of the drive's power electronics, the drive is able to absorb this additional energy flow as the damping power supplied by the VSD is a small component when compared to the overall system power, this corresponds to additional studies on VSD based systems [26,27].

When looking at the blue waveform in Figure 60, a small amount of torque is supplied in relation to the speed variation. This leads to a smaller disturbance peak in each cycle of the oscillation as energy is dissipated. A small amount of power is being dissipated in the system due to the small torque component. With a small torque reference applied, the torque peaks decrease slightly with each cycle resulting on the system taking a longer time to settle and return to a stable state.

When observing the scenario featuring the green waveform in Figure 60. The torque supplied to the reference is the same as the speed variation. With the increased torque, more power is being dissipated when compared to the second scenario. This increase in energy dissipation results in smaller disturbance peaks following each cycle. With each oscillation cycle, the torque supplied is equal to the speed variations peak in that cycle such that, a larger amount of power is being dissipated leading to a much smaller disturbance peak in the cycle that follows.

As a result of the increased torque component, the power being dissipated shown in the third scenario is greater than the power dissipated when compared to the second scenario. With a changing torque requirement in each cycle, the VSD supplies a modulating torque as the torque requirement is different in each oscillation cycle as the torque peaks are lowered from dissipated energy. The waveforms in Figure 60 can be summarized such that by increasing the torque component, increased damping is achieved. With supplying a torque component of equal magnitude to the speed variation, the best damping scenario is achieved.

11.1 Discussion of the Research report objectives

To reiterate the research objectives outlined in Section 1.1, the research question are once again presented. The research objectives are:

- ➢ Can a VSD provide damping for oscillations associated with its mechanical load?

- ➢ What types of mechanical oscillation can be damped?

- ➢ Will providing damping have a detrimental effect on the VSD-mechanical load performance?

With the simulation completed, three observations can be obtained. The first observation and answering the first question presented, can a VSD provide damping for oscillations associated with its mechanical load? The simulation has shown that a VSD is capable of providing a damping torque for oscillations associated with mechanical loads with an increase in damping occurring with an increasing torque. This increase in damping was demonstrated in Figures 55 and 57.

The second observation and answering the second question, what type of oscillations can be damped? The VSD is able to counter specific oscillations. In the discussion, the oscillating disturbances in the system originated from a single torque pulse being injected into the load. Such an example would be the clamping and releasing of the shaft for a second with example of the torque pulse applied shown with Figure 50.

The third observation and answering the final question, will the damping provided have a detrimental effect on system performance? The VSD implemented in the system acts as the damper element in the system. When the dampening torque is supplied, the system maintained the 200 Nm reference level as the torque disturbance is minimized and no adverse power fluctuations were observed from the simulation. This can observed in the superposition of the various transmitted torques with different levels of damping torque supplied, as shown in Figure 58.

12 Future work

The research project investigated via a literature survey and by mathematically modeling shaft elements that it is possible to simulate a VSD providing a damping torque to counter mechanical oscillations in the system as a result of a torque pulse introduced into the load. With the theoretical component in hand, a goal set for future work would be to replicate the simulation results in a lab setting. The lab setup would include a small scale setup such as a 5.5 kW drive with a VSD sized for the motor. The lab setup would also need to incorporate a mechanical shaft model with a low Moment of Inertia component as was indicated in the simulation pre-calculation such that an observable shaft oscillation can be achieved.

13 Conclusion

A literature survey and case study was done to investigate how a VSD provides a damping torque during a mechanical disturbance. From first principles, an electrical and mechanical system was described. From the discussion, it was shown how an electrical system translates to a mechanical rotational system. It then determined how voltage and current translated into speed and torque respectively for such a system.

It was determined that during a speed variation, the VSD applying a torque with the speed variation provides a damping effect. The VSD provides a damping torque by monitoring the speed variation, and injects a current into the system to provide the torque component. As the speed variation is never constant, as was seen from the decaying oscillating torque and speed variation. The damping torque provided by the VSD is also required to vary accordingly and can be best described as a modulating torque.

A discussion then followed onto how the VSD drive acts as the damper element in a wind turbine generation model. It was found that the drive needs only to provide a small correction signal to provide a damping torque.

A simulation then followed that demonstrated that by the VSD applying a torque ripple corrective signal based on the speed variation. The drive is able to provide a modulating torque component to offset the torque oscillation disturbance in the system.

The VSD using DTC, provides complete control over the torque and flux of the motor. In the simulation, the VSD is able to provide a modulation torque as the result of a shaft oscillation occurring from a torque pulse. This modulating torque provided by the drive has an advantage of extending the life span of mechanical systems in large drive setups.

References

[1] S. Schramm, J. Song-Manguelle, P. Rotondo, and C. Sihler, "Damping Torsional Interharmonic Effects of Large Drives*, "IEEE Transactions on Power Electronics*," vol. 25, no. 4, pp. 1090-1098, April 2010.

[2] A. Dutka and M. Orkisz, "Analysis and remedies for torsional oscillations in rotating machinery*, "IEEE International Symposium on Power Electronics & Drives*," pp. 474-481, September 2011.

[3] K. Anderson, "Torsional Oscillations in Drive systems*," in the *Cement Industry Technical Conference*, Conference road, pp. 124-150, May 2005.

[4] B. Dury, "The Control Techniques Drives and Control Handbook, 2nd edition," Published by *the Institute of Engineering and Technology*, London, United Kingdom, chapter B8, pp. 441-447, 2009.

[5] D.Jones, "Invertek Drives. OptiDrive Advanced Technical Manual, Revision 1.04," pp. 32-52, 2002. https://www.anaconsystems.com/data/manual.pdf

[6] "Schneider Electric Technical Publications," *Cahier Technique Schneider Electric* no. 208 / pp. 25, November 2003.

http://www2.schneider-electric.com/documents/technical-publications/en/shared/automation/automation-information-networks/ect208.pdf

[7] Amit Abraham, Schneider Electric. South Africa, Personal Communication.
Contact details: amitabraham15@gmail.com, Mobile: 082 581 7915.

[8] Kiru Govender, Afrilek Automation. South Africa, Personal Communication.
Contact details: kiru@afrilek.com, Mobile: 083 775 0449.

[9] David Klein, Buhler, Switzerland. Automation Engineering Team Leader.
Personal Communication.
Contact details: david.klein@buhlergroup.com, Contact line: +41 719 55 2759.

[10] Bruno Dietschweiler, Buhler. Switzerland. Automation Engineering Drive Specialist.
Personal Communication.
Contact details: bruno.dietschweiler@buhlergroup.com, Contact line: +41 719 55 3365.

[11] T. Feese and R. Maxfield, "Torsional vibration problem with motor/ID fans due to PWM variable frequency drive*," Proceedings of the thirty-seventh Turbo machinery symposium*, pp. 45-56, 2008.

[12] N. Mohan, "Advanced electric drives. Analysis, control and modeling using Simulink*,"* Published by *MNPERE*, P.O Box 14503, Minneapolis, MN 55414, USA, pp. 28-35, 2014.

[13] N. Mohan, "Advanced electric drives. Analysis, control and modeling using Simulink," Published by *MNPERE*, P.O Box 14503, Minneapolis, MN 55414, USA, pp. 60, 2014.

[14] Mathworks. *Simulation of an AC Drive.*

http://www.mathworks.com/help/physmod/sps/powersys/ug/simulating-an-ac-motor-drive.html

[15] K. Suman, K. Suneeta, and M. Sasikala, "Direct Torque Controlled Induction Motor Drive with Space Vector Modulation Fed with Three-level Inverter," *IEEE International Conference on Power Electronics, Drives and Energy Systems,* pp. 1-6, December 2012.

[16] A. Moodadla and V. Nandiraju, "Modelling and Simulation of SVPWM based vector controlled HVDC light systems," *Electrical Engineering Department, National Institute of Technology-Warangal*, Pradesh, India. http://lejpt.academicdirect.org/A21/023_036.htm

[17] D. Casadei, G. Serra, and K. Tani, "Implementation of a Direct Torque Control Algorithm for Induction Motors Based on Discrete Space Vector Modulation," *IEEE Transactions on Power Electronics*, vol. 15, vo. 4, pp. 769-777, July 2000.

[18] J. Van Coller, "Variable Speed drives for AC Machines ELEN 7048*," University of the Witwatersrand, School of Electrical and Information Engineering*, pp. 113-114, 2013.

[19] R. Serway and J. Jewett, "Physics for Scientists and Engineers, 6th Edition," *Thomson/Brooks-cole Publishing*, chapter 32, pp. 1026-1033, 2003.

[20] N. Nise, "Control Systems Engineering, 2nd Edition," Published by The *Benjamin/Cummings Publishing Company Inc.,* pp. 71-72, 1995.

[21] S. K. Bhattacharya, "Control Systems Engineering, 2nd Edition," Published by *Pearson Education*, pp. 13-22, 2008.

[22] T. Burton, N. Jenkins, D. Sharpe, and E. Bossanyi, "Wind Energy Handbook 2nd Edition," *A John Wiley and Sons, Ltd.,* chapter 6*, pp. 360-36, 2011.*

[23] T. Burton, N. Jenkins, D. Sharpe, and E. Bossanyi, "Wind Energy Handbook 2nd Edition," *A John Wiley and Sons, Ltd.,* chapter 7*, pp. 442-443, 2011.*

[24] G. Mandic, E. Ghotbi, A. Nasiri, F. Oyague, and E. Muljadi, *"*Mechanical Stress Reduction in Variable Speed Wind Turbine Drivetrains*," IEEE Energy Conversion Congress and Exposition*, pp. 306-312, September 2011.

[25] T. Burton, N. Jenkins, D. Sharpe, and E. Bossanyi, "Wind Energy Handbook 2nd Edition*," A John Wiley and Sons, Ltd.,* chapter 8, *pp. 492-507, 2011.*

[26] L. Chen, H. Xu, and J. Wenske, "Active damping of torsional vibration in the drive train of a DFIG wind turbine*," International conference on renewable energies and power quality*. April 2014*.*

[27] N. Lad, C. Hempsted, G. Driessen, J. Quillan, and S. Zhon, "*Study of a damped torsional pendulum driven into resonance," pp. 1-4, 2013.*
http://www.homepages.ucl.ac.uk/~zcapnla/Images%20&%20PDFs/NX3_Lad_N.pdf

Appendix

The copyright clearance certificates and respective written E-mail permissions for figures used are listed.

Copyright clearance certificate **Figures 1 and 2.**

Copyright clearance certificate **Figures 3 and 4.**

Figures 7,8 and 9. **Table 4.1**

Written E-mail from publisher allowing permission.

Drollinger, Ashton M <ashton@turbo-lab.tamu.edu>
to Benjamin, me

Mr. Blaski,

Please be sure to accurately state that you are using the figures and tables from a paper published at the 37th Turbomachinery Symposium and you have permission to use them.

Thank you,

Ashton Drollinger
Publications Coordinator
Turbomachinery Laboratory
PH: 979-458-2808

Join our Mailing List

Copyright clearance certificate **Figures 11,12,13,14,15 and 16.**

Copyright clearance certificate **Figure 19.**

Copyright clearance certificate **Figure 21**

Copyright clearance certificate **Figures 24,25,26,27,28 and 29.**

Copyright
Clearance
Center

Back to view orders

Copy order

Confirmation Number: 11566453
Order Date: 05/31/2016

Customer Information

Customer: Greg Blaski
Account Number: 3001032709
Organization: Greg Blaski
Email: skarnkai@gmail.com
Phone: +27 119020001

Search order details by: Choose One ▼   Go

This is not an invoice

Order Details

Physics for scientists and engineers, with modern physics

Billing Status:
N/A

Order detail ID:	69754030	
ISBN:	978-0-534-40844-2	
Publication Type:	Book	
Publisher:	THOMSON-BROOKS/COLE	
Author/Editor:	SERWAY, RAYMOND A. ; JEWETT, JOHN W.	

Permission Status: ✅ Granted

Permission type: Republish or display content
Type of use: Republish in a thesis/dissertation
     Order License Id: 3879370886068

Hide details

Requestor type	Academic institution
Format	Print
Portion	chart/graph/table/figure
Number of charts/graphs/tables/figures	6
Title or numeric reference of the portion(s)	Chapter 32, Figure 32.16. Chapter 32, Figure 32.17. Chapter 32, Figure 32.18. Chapter 32, Figure 32.22. Chapter 32, Figure 32.23. Chapter 32, Figure 32.19.
Title of the article or chapter the portion is from	N/A
Editor of portion(s)	N/A
Author of portion(s)	N/A
Volume of serial or monograph	N/A
Issue, if republishing an article from a serial	N/A
Page range of portion	1015-1022
Publication date of portion	31.05.2016
Rights for	Main product and any product related to main product
Duration of use	Current edition and up to 5 years
Creation of copies for the disabled	no
With minor editing	

privileges	no
For distribution to	United States
In the following language(s)	Original language of publication
With incidental promotional use	no
Lifetime unit quantity of new product	Up to 499
Made available in the following markets	Education
The requesting person/organization	Greg Blaski
Order reference number	
Author/Editor	Greg Blaski
The standard identifier	Engineering
Title	Investigation into the use of variable speed drives to damp mechanical oscillations
Publisher	University of the Witwatersrand
Expected publication date	Jun 2016
Estimated size (pages)	65

Note: This item was invoiced separately through our **RightsLink service.** More info $ 0.00

Total order items: 1	**Order Total: $0.00**

Copyright clearance certificate **Figures 37,38,39,40,41,43,44 and 46**

JOHN WILEY AND SONS ORDER DETAILS

May 31, 2016

Order Number	501146928
Order date	May 29, 2016
Licensed Content Publisher	John Wiley and Sons
Licensed Content Publication	Wiley Books
Licensed Content Title	Wind Energy Handbook, 2nd Edition
Licensed Content Author	Tony Burton, Nick Jenkins, David Sharpe, Ervin Bossanyi
Licensed Content Date	May 1, 2011
Pages	780
Type of use	Dissertation/Thesis
Requestor type	University/Academic
Format	Print
Portion	Figure/table
Number of figures/tables	8
Original Wiley figure/table number(s)	Figure 6.20, Figure 7.32, Figure 7.37, Figure 6.19 (c), Figure 6.19(d), Figure 7.38, Figure 8.5 and Figure 8.13
Will you be translating?	No
Title of your thesis / dissertation	Investigation into the use of variable speed drives to damp mechanical oscillations
Expected completion date	Jun 2016
Expected size (number of pages)	65
Requestor Location	Greg Blaski N/A N/A N/A N/A, South Africa 2000 Attn: Greg Blaski
Total	0.00 USD

Copyright clearance certificate **Figure 42.**